

Received 9 November 2022, accepted 1 December 2022, date of publication 6 December 2022,  
date of current version 29 December 2022.

Digital Object Identifier 10.1109/ACCESS.2022.3227217

## TOPICAL REVIEW

# A Systematic Review of Dynamic Wireless Charging System for Electric Transportation

YUVARAJA SHANMUGAM<sup>1</sup>, NARAYANAMOORTHY R<sup>1</sup>, PRADEEP VISHNURAM<sup>1</sup>,  
MOHIT BAJAJ<sup>2,3</sup>, KAREEM M. ABORAS<sup>4</sup>, PADMANABH THAKUR<sup>2</sup>, AND KITMO<sup>5</sup>

<sup>1</sup>Electric Vehicle Charging Research Centre, Department of Electrical and Electronics Engineering, SRM Institute of Science and Technology, Chennai 603203, India

<sup>2</sup>Department of Electrical Engineering, Graphic Era (Deemed to be University), Dehradun-248002, India

<sup>3</sup>Graphic Era Hill University, Dehradun, 248002, India

<sup>4</sup>Department of Electrical Power and Machines, Faculty of Engineering, Alexandria University, Alexandria 21526, Egypt

<sup>5</sup>Department of Renewable Energy, National Advanced School of Engineering of University of Maroua, Maroua, Cameroon

Corresponding authors: Narayanamoorthy R (narayanamoorthy.r@gmail.com), Mohit Bajaj (thebestbajaj@gmail.com), and Kitmo (kitmobahn@gmail.com)

**ABSTRACT** Green electricity and green transportation are the primary requirements for smart cities. Maximizing EV utilization is the key requirement in the development of green transportation. However, EV technology faces challenges due to the long battery recharging time and heavy batteries to achieve extended driving ranges. Different approaches are investigated to charge the EV by battery swapping, plugin, or wireless. Recently the wireless charging approach is gaining popularity because of safety, extended driving range, dynamic charging, and human intervention-free recharging. However, multiple factors need to be considered in the design of the WPT system and require expertise in different domains. This paper discusses a systematic approach on the various parameters involved in a dynamic wireless charging system design. The major functional units in WPT such as charging couplers, compensation network, and power inverters topologies are addressed. Additionally, this paper discusses the issues involved in grid-tied and renewable integrated dynamic charging systems. Moreover, the step-by-step procedure is described to understand the process involved in the dynamic charging system design. Finally, various case studies at different power levels are presented to get more insights into practical design.

**INDEX TERMS** Inductive charging, dynamic charging, electric vehicle, charging couplers, in-motion charging.

### ABBREVIATIONS

EV	Electric Vehicle.
GHG	Green House Gas.
SWC	stationary wireless charging.
DWC	Dynamic Wireless Charging.
IPT	Inductive Power Transfer.
KRRI	Korean Rail Road Research Institute.
ORNL	Oak Ridge National Laboratory.
OLEV	On-Line Electric Vehicle.
SUV	Sports Utility Vehicle.
KAIST	Korea Advanced Institute of Science and Technology.

FOD	Foreign Object Detection.
PV	Photo Voltaic.
CP	Circular Pad.
RP	Rectangular Pad.
DDP	Double D-Pad.
DDQ	Double D Quadrature Pad.
BP	Bipolar Pad.
SS	Series-Series.
SP	Series-Parallel.
PS	Parallel-Series.
PP	Parallel-Parallel.
HF	High frequency.
a.c.	alternating current.
d.c.	direct current.
DPC	Direct Power Control.

The associate editor coordinating the review of this manuscript and approving it for publication was Wei Xu<sup>1</sup>.

MOD	Metal Object Detection.
LOD	Living Object Detection.
ZVS	Zero Voltage Switching.
ZPA	Zero Phase Angle.
CC	Constant Current.
CV	Constant Voltage.
SoC	State of Charge.
RES	Renewable Energy Sources.
V2G	Vehicle to Grid.
ESS	Energy storage system.
SAE	Society of Automotive Engineers.
EMI	Electromagnetic interference.
EMC	Electromagnetic compatibility.

## I. INTRODUCTION

A Market for EV is increased rapidly by 168% globally in 2021 to decrease the emission of GHG. The usage of EVs on road transportation protects the environment from GHG emissions. During the year 2020, higher than 500 lakh tones of CO<sub>2</sub> equivalent GHG emissions were reduced by EVs [1].

The development of charging infrastructure should increase proportionately to the EVs market. The requirement for automotive lithium-ion energy storage elements is also increased to overcome the EVs market demand. Battery swapping, conductive, and inductive charging are energizing EV storage devices [2]. A battery swapping system for an EV is a charging method in which a drained battery is swapped with a fully charged battery. The different types of battery swapping are sideways, rear, and bottom [3]. A vehicle may alert the information system that it needs a battery swap when the battery is dead. The charging station will get the information from the EV through wave communication about EVs position, estimated arrival time, and identifications so that the battery is ready when the vehicle arrives at the station. When the EV arrives at the station, the computer system finds the pertinent information associated with the EVs membership card. The charging station's operator will confirm the information and guide the EV to the swapping zone, where the necessary battery change will be performed using an automatic arm system [4]. In conductive charging, mechanical conductors are used to transmit electricity to the battery of the EV. Thus, it is more effective. These technologies have two categories: a.c. and d.c., depending on how EV batteries are linked to the grid.

Furthermore, the charging method is classified into two types based on charger arrangement [5]: onboard charging, where the charger is mounted within the vehicle, and off-board charging, where the charger is deployed outside the vehicle. Off-board chargers might be rapid chargers whilst on-board chargers are often slow ones. The power flow in the chargers may be unidirectional or bidirectional. The battery must be linked to the earth throughout the charging process, regardless of whether the EV body includes onboard or off-board. When there is no physical barrier between the charger and the battery, isolation monitoring is essential. A fast-charging station [6], [7] proposed to charge an EV up to 80%

SoC within 30 minutes of charging time. The CHAdeMO group recently unveiled a new charging methodology. The power rating is increased, such as d.c. They are charging with more than 500 kW power with 600 A maximum current.

Additionally, they suggest liquid cooling and a proper locking mechanism for connectors [5]. Due to the nonlinear nature of EV load, EV load penetration in the grid causes a considerable voltage deviation, an increase in losses of the transformer, peak demand, and a higher order harmonics distortion in current. The distribution side equipment's lifetime will decrease due to these issues. ESS [8] may reduce these effects by using a fast-charging station V2G design to shape the peak demand with few extra facilities. Additionally, grid problems associated with fast charging may be mitigated by integrating RES into the distribution grid [9].

The battery swapping and conductive charging systems are driver-dependent on the charging process and require bulk energy storage devices. The dependency of the driver can be overcome by inductive charging. The different types of inductive charging systems are stationary and dynamic charging systems. The inductive charging system during driving conditions (DWC System) is used to reduce the requirement for a high-volume energy storage device, the vehicle's weight, and extends the vehicle's driving range. Because of the frequent charging infrastructure built under highways, dynamic charging enables smaller and lighter energy storage devices to be employed. Despite the knowledge that the DWC needs more investments in electrical lines rather than static charging, smaller batteries with longer battery life might save more costs for the system. The researchers from KAIST demonstrated these advantages with the help of OLEV. When the dynamic charging system is used instead of stationary, the overall cost is estimated to be reduced by 20.8% [10]. The barriers to battery swapping are inadequate standardization among EV batteries, increased number of batteries required to power the same number of EVs, shorter commercial life of battery packs due to customer preference for new batteries with more excellent range, and higher life-cycle expenses of battery leasing [11]. A long track is embedded on the roadside, and the receiver pad(s) is positioned under the vehicle in a DWC system. The track embedded on the roadside might be a long continuous track or continuous segmental charging pad [12]. The receiver pad which is installed under the vehicle initiates the charging process whenever it is positioned over the transmitter track. The control of the energizing process of a long track is simple, but the power loss due to a portion of the non-interactive track is high. The energization process of the segmental pad structure is complex. Still, the particular pad is energized only during the receiver pad is positioned over it, and the remaining pads are in ideal condition. There are several organizations from various countries that are analyzing the DWC system. The University of California from Berkeley successfully developed and demonstrated the 60 kW IPT charging system on behalf of California PATH [14]. A 100 m long track was installed with a 50 kW powered IPT charging system under project VICTORIA. The DWC

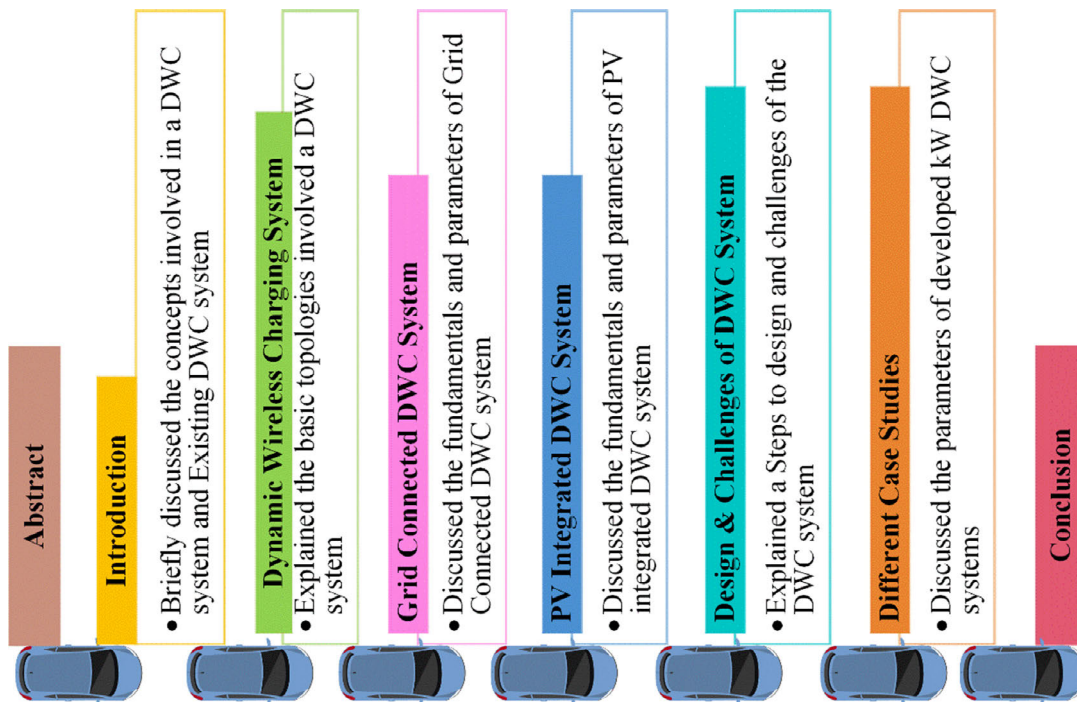


FIGURE 1. Overall structure of review article.

system was successfully demonstrated with the help of a 20-kWh lithium-ion energy storage device. The dimension of the receiver coil was designed to be higher than the transmitter coil to be comfortable with static IPT and dynamic IPT charging systems [15]. The German government installed the 200-kW IPT charging system with the help of Bombardier PRIMOVE and energized the Electrified public transport system speedily [16]. A 128 m, 1 MW, 60 kHz IPT charging system for a high-speed Electric train was successfully demonstrated by KRRI [17]. ORNL researchers developed a 120 kW DWC system, and the power transfer efficiency is 97% with a 15.24 cm air gap between charging couplers [18]. A 60 kW DWC system for an OLEV bus and a 20 kW DWC system for SUV were designed and demonstrated by KAIST with higher than 70 % power transfer efficiency [19].

The structure of this review article is represented in fig. 1. In this article, the significant components of the DWC system, challenges involved in the DWC system, Grid-tied DWC system, and PV-integrated DWC system are discussed. The components of the DWC system are charging couplers (transmitter and receiver), Impedance matching networks (transmitter-side and receiver-side), Power Modulators (transmitter-side and receiver-side), Sensing Unit (FOD and Vehicle Position), and a Controller Unit. The charging couplers are used to transmit and receive power based on IPT technology. The impedance matching network is used as a compensator and assists the couplers in attaining resonant conditions. The maximum power is transferred between charging couplers during this resonant condition. The power

modulators convert the a.c.-d.c. or d.c.-a.c. on the receiver or transmitter sides, respectively.

Based on the transformer working principle, the transmitter is considered the primary side, and the receiver is the secondary side of the IPT system. The parameters involved in wireless charging are the systems' operating frequency, alignment of charging couplers, the geometry of the charging coupler, selection of proper resonant network, and the system power. The factors involved in the design of charging couplers are inductance parameters, rated power level, airgap distance, proper ventilation, and interoperable characteristics. The weight of the receiver pad should be within the permissible value. The factors involved in the compensation network are maintaining the resonant frequency during the misalignment and transferring the maximum power. The selection of compensation network elements is based on these conditions. The selection of inverter is based on power level and operating frequency. The DWC system impacts the operational parameters of the utility grid, such as voltage instability, harmonics, and sudden transients during the charging process. The sudden rise in a utility grid by the DWC process generates voltage instability problems and improper demand curves. Many transportation-related systems rely on solar energy for their power source. A grid-integrated photovoltaic array will be installed in an EV charging station. Depending on the different parameters, the charging methodologies might be wired or wireless. Additionally, there are many systems operated by photovoltaic sources. An independent solar-powered road surveillance system is proposed to detect moving vehicles

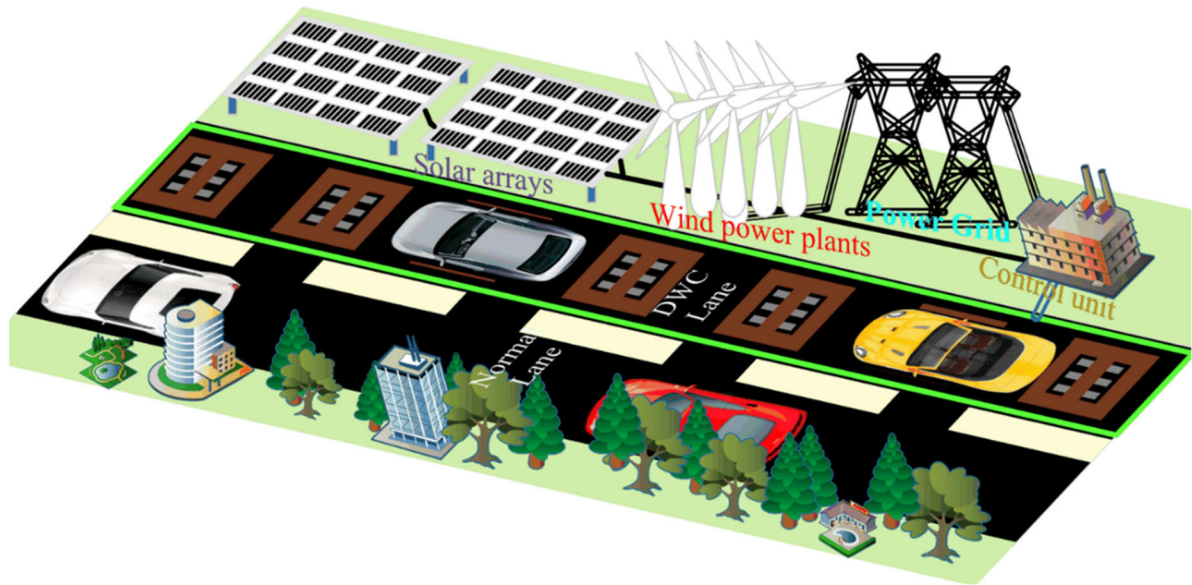


**FIGURE 2.** Renewable energy integrated grid-tied DWC System.

that exceed the speed limit and report them. The integrated solar energy assists the grid system in achieving a smooth peak demand profile and decreasing the grid utility cost. The essential representation of the renewable energy integrated grid-tied DWC system is shown in fig. 2.

## II. DYNAMIC WIRELESS CHARGING SYSTEM

The DWC system is an in-motion charging system for EVs. The transmitter track contains multiple transmitter pads that are positioned along the roadside. The receiver pad is positioned under the vehicle with an allowable ground clearance level. The main components of the DWC system are Charging pads (Ground-side transmitter pad and vehicle-side receiver pad), a Compensation network, and Power Modulators to control the input and output power. Table 1, Table 2, and Table 3 represent the factors of the different coil, compensation, and power inverter topologies, respectively.

### A. CHARGING COUPLERS

The charging couplers are an essential part of the DWC system. The transmitter and receiver pad structures can be classified by their production of flux direction. A Vertical or horizontal flux-producing coil is considered a non-polarized coil. A Vertical and horizontal flux-producing coil is considered a polarized coil [20]. The non-polarized coils are circular, square, rectangular, and hexagonal. A single-shaped coil produces the charging flux in a charging pad. The polarized coils are DDP, DDQP, BP, tripolar, and Quadrupole. The charging flux is produced by more than one coil in a single charging pad. The charging couplers are loosely coupled, and the air is a medium for transferring power. The leakage inductance between the loosely coupled charging couplers is higher than the magnetizing inductance of the couplers.

Normally, CP is preferable in stationary charging and not suitable for dynamic charging. The design of CP is compact and simple.

Additionally, the absence of corners in CP reduces the eddy current and low leakage flux for the CP receiver. But CP is unsuitable for In-motion charging due to lateral and longitudinal movements [21]. A flux pipe coil is proposed to increase lateral misalignment tolerance and coupling factor. But the intercepting flux by shielding affects the quality factor [22]. An RP is remedying the problems associated with CP and flux pipe. The transmission efficiency of the RP is high, and the required area and mass of the coil are low. But the stray magnetic field of the pad is high, and the flux density of the core is low. DDP can avoid these problems. It has half of the stray magnetic field compared with a rectangular pad, and the degree of freedom for magnetic coupling is high [23]. An additional quadrature pad is added with a double D-pad to increase the power transfer efficiency. This decoupled quadrature coil can eliminate the null point of the DDP [24]. The required volume of coil for the DDQP is high. BP can reduce it. A misalignment tolerance of the BP is better than other proposed pads [25]. The RP, DDP, and BP are more suitable on the transmitter side, and BP and DDQP are suitable on the receiver side.

For a single coil IPT system, the uncompensated power  $P_{su}$  is given by the multiplication of open circuit voltage ( $V_{oc}$ ) and short circuit current ( $I_{sc}$ ) in (1) [26]

$$P_{su} = V_{oc} \times I_{sc} = \omega_r \frac{M^2 I_{pr}^2}{L_s} \quad (1)$$

where,  $\omega_r$ ,  $I_{pr}$ ,  $M$ ,  $L_s$  denotes the angular resonant frequency, resonant current at the primary side, mutual inductance between the transmitter and receiver coil, and secondary side inductance, respectively. Additionally, the output power of



the dual coil pad system can be calculated by adding the power of two coils [27].

$$\text{For coil 1, } V_{oc1} = \omega_r (M_{p1s1} + M_{p2s1}) I_{pr1} \quad (2)$$

$$\text{For coil 2, } V_{oc2} = \omega_r (M_{p1s2} + M_{p2s2}) I_{pr2} \quad (3)$$

$$\text{For coil 1, } I_{sc1} = \frac{V_{oc1}}{\omega_r L_{s1}} = \frac{(M_{p1s1} + M_{p2s1}) I_{pr1}}{L_{s1}} \quad (4)$$

$$\text{For coil 2, } I_{sc2} = \frac{V_{oc2}}{\omega_r L_{s2}} = \frac{(M_{p1s2} + M_{p2s2}) I_{pr2}}{L_{s2}} \quad (5)$$

$$\text{Total, } P_{su} = \left( \frac{(M_{p1s1} + M_{p2s1})^2 I_{pr1}^2}{L_{s1}} + \frac{(M_{p1s2} + M_{p2s2})^2 I_{pr2}^2}{L_{s2}} \right) \omega_r \quad (6)$$

The SAE suggested that the operating frequency of the DWC system is 85 kHz [28]. The skin effect and proximity effects are high in this HF range. The usage of Litz wire can reduce these losses significantly. The total power loss of the core per unit volume when the magnetic materials are experiencing the external dynamic magnetic field can be calculated by using Steinmetz's equation (7) [29].

Average power loss per unit volume in mW per cm<sup>3</sup>,

$$P_v = k f^a B^b \quad (7)$$

where k, a and b are Steinmetz's co-efficient, f is system frequency, and kHz and B are the peak magnetic flux density of the core. Generally, ferrite material is used for a core, and aluminum material is used for shielding. The magnetic field emission exposure limits are standardized by ICNIRP [30].

### 1) INFERENCES

WPT charging coupler requirements include high misalignment tolerance, interoperability, high power transfer efficiency with low cost and less weight, efficient thermal management, and SAE and ICNIRP recommendations. It is essential to optimize the charging coupler to develop a suitable construction. The weight of the Litz wire, ferrite bars, and aluminum increases in direct proportion to their dimension. Therefore, the coupler structure must be adequately developed. The height of the flux path depends on the dimension of the charging pad.

- The circular, square, hexagonal, and rectangular non-polarized pads are appropriate for stationary WPT charging. Polarized pads like DD, DDQ, and BP are ideal for dynamic WPT charging.
- The maximum efficiency will be transferred through charging couplers when the outer dimensions of the couplers are equal.
- High misalignment tolerance is provided by the BP and DDQ pads, however, this needs effective decoupling between pads and complex converter control to energize the pads.

- High-power WPT charging requires efficient shielding. The materials such as aluminum, ferrite, and Mu metal will be considered to design the shielding.
- The spacing between the turns of the charging coil and the gap between the charging coil and the shielding must be tuned to minimize the capacitance's influence.

### B. COMPENSATION NETWORK TOPOLOGIES

The network consisting of a passive element assisting the charging pads in transferring maximum power during misalignment conditions is called a compensation network or impedance matching network. The apparent minimizing power and maximizing power transferring capability of the charging pad. The network consists of only one mono-resonant capacitor, and more than one capacitor combined with an inductor is considered a multi-resonant network [31]. A series compensation where the capacitor is connected with the charging pad is suitable for long distributed tracks, and A parallel compensation where the capacitor is connected in parallel with the charging pad is suitable for concentrated winding pads and high current systems. The basic mono-resonant topologies are SS, SP, PP, and PS concerning transmitter-receiver. The transmitter-side capacitance ( $C_T$ ) of the basic topologies is represented using transmitter pad self-inductance ( $L_T$ ), receiver pad self-inductance ( $L_R$ ), the resonant frequency ( $\omega_r$ ), and mutual inductance (M) [32]

$$C_{T\_SS} = \frac{1}{\omega_r^2 L_T} \quad (\text{for SS topology}) \quad (8)$$

$$C_{T\_SP} = \frac{1}{\left(L_T - \frac{M^2}{L_R}\right) \omega_r^2} \quad (\text{for SP topology}) \quad (9)$$

$$C_{T\_PS} = \frac{L_T}{\left(\frac{\omega_r^2 M^2}{R}\right)^2 + \omega_r^2 L_T^2} \quad (\text{for PS topology}) \quad (10)$$

$$C_{T\_PP} = \frac{L_T - \frac{M^2}{L_R}}{\left(\frac{M^2 R}{L_R}\right)^2 + \left(L_T - \frac{M^2}{L_R}\right)^2 \omega_r^2} \quad (\text{for PP topology}) \quad (11)$$

where T and R represent the transmitter side and receiver side of the charging couplers. The efficiency of the transmitter side coil ( $\eta_T$ ) and receiver side coil ( $\eta_R$ ) can be represented using reflected impedance ( $Z_{reflected}$ ) from the receiver to the transmitter [33].

$$\eta_T = \frac{\text{Re}(Z_{reflected})}{R_{T\_eq} + \text{Re}(Z_{reflected})} \quad (12)$$

$$\eta_s = \frac{\text{Re}(Z_R) - R_{R\_eq}}{\text{Re}(Z_R)} \quad (13)$$

$$Z_{reflected} = \frac{\omega_r^2 M^2}{Z_R} \quad (14)$$

The receiver side total impedance,  $Z_T$  is given in (15)

$$Z_r = j\omega_r L_R + \frac{1}{j\omega_r C_s} + R_{R\_eq} + R_L \quad (15)$$

where  $R_{T\_eq}$  and  $R_{R\_eq}$  represent the equivalent resistance concerning transmitter and receiver, the multi-resonant topologies such as LCC, LCL, SP, and LCCL are formed by combinations of passive elements. Among these topologies, the LCC and LCL are used to achieve more than 95% at a particular point.

### 1) INFERENCES

The WPT system can accomplish CC/CV output, total impedance control, maximum transfer during misalignment, and smooth switching operations with the help of the compensation circuits. Mono-resonant networks may be used for stationary WPT, whereas double-sided LCC/LCC can be used for dynamic WPT. High input current is needed for the PS and PP network and low d.c. link voltage is needed for the SP and SS network. The LCC/S and LCC/SP networks provide more design flexibility and smooth ZVS operation. The LCCC/LCCC network employs a fast and precise tuning technique. The addition of excess passive elements in the compensation network to smoothen the operation may create a circulating current in the adjacent pads.

- The design of the compensation network concerns load variations and misalignment conditions.
- The design of the compensation network depends on the inverter's rating.
- High-frequency inductors with ferrite cores and capacitors are required for compensating network design.

### C. POWER CONVERTER TOPOLOGIES

A flow of power to energize and de-energize the transmitter coils is controlled by an HF high-power inverter. Inverters can energize a single transmitter coil or multiple transmitter coils simultaneously. Additionally, the power converter is used on the receiver side to provide constant d.c. to the energy storage device. The inverter should have low switching losses. By utilizing soft-switching combined with the compensation networks, switching stress can be reduced. An HF pulse must be generated by the driver circuit of the inverter based on the vehicle position. It is feasible to achieve high power and HF with wide band gap GaN and SiC switches because they have low on-state resistance and high-temperature co-efficient. A conventional H-bridge inverter [34], [35], [36] is used to drive DWC coils embedded in the road. The number of switches is constant irrespective of the number of charging couplers. Despite the simple switching control, a single resonant inverter is required for all coils, which increases the switches' power rating and the operation's complexity. Alternatively, The N number of coils is energized by the N number of conventional H-bridge inverters [37], [38], [39]. This will increase the size and cost of the system and drive the switches. Multiple switching patterns are required. The N-legged inverter is proposed [12], [13] to limit the number of switches concerning the charging couplers. But, the control complexity of this inverter is high. The fea-

tures of the different types of primary side power converters are represented in the table. The instantaneous output voltage,  $V_o$  of the conventional H-bridge inverter is mentioned in (16) [40]

$$V_o = \sum_{n=1,3,5,\dots}^{\infty} \frac{4v_s}{n\pi} \sin n\omega t \quad (16)$$

where  $v_s$  is the input voltage and RMS value of the fundamental component,  $v_{o1} = \frac{4v_s}{\sqrt{2\pi}} = 0.9v_s$  and  $v_{on}$  is the RMS value of the  $n^{\text{th}}$  harmonic component. Total harmonic distortion,

$$\text{THD} = \frac{1}{v_{o1}} \left( \sum_{n=2,3,\dots}^{\infty} v_{on}^2 \right)^{0.5} \quad (17)$$

### 1) INFERENCES

The charging pads of the WPT system are driven by power converters. The considerations of power converter design are current and voltage rating, and the number of charging pads. The output of the HF high-power inverter is fed to the charging pad through the compensation network. The power rating and operating frequency of the system are the factors in the choice of power semiconductor switches, The controller can produce the driving pulses for the switches. The detection circuit provides input to the controller. The driving pulse generation of the converter needs to be synchronized to suit vehicle speed.

- The concerns of the power inverter are smooth energization of charging couplers, reduced switching stress and losses, and simple control algorithms.
- The considerations of high-power HF inverters are compactable (may experience EMI issues due to lengthy connections), reduced harmonic injections, and active protection circuits.

### D. FOREIGN OBJECT DETECTION

Power is transferred from the coils embedded on the road to the receiver coil whenever the coil is placed over it through the air medium. The high magnetic field generated by the transmitter coil will transfer the power to any metal object or living object placed on the coil instead of the receiver coil [41]. A sufficient object mass will allow the rated power to flow through it. In worst-case scenarios, heat and fire may be generated when the transferred power circulates in the objects. Additionally, the inductance parameters of the coil are disturbed by the introduction of the foreign object. So, it is necessary to integrate the foreign object detection system with the DWC system to detect the availability of foreign objects on the charging pads. The detecting mechanism helps the charging system avoid foreign object-induced efficiency losses and temperature increases. Depending on the power level and detecting objects, FOD can be classified as MOD and LOD [42]. Field-based detection, wave-based detection, and system parameters can also be used to classify FOD.

Systems with low-rated power usually use the system parameter detection method, while the high-power-rated system uses the other two methods. Due to the large air gap in a high-power system (i.e., the power transferring distance is proportional to the operating system power), the LOD applies to those systems. The system parameters method relates to non-electrical parameters such as temperatures and pressure and electrical parameter such as eddy current. Hence, sensors measure the changes in pressure and temperature on the charging pad due to metal objects. But these sensors failed to differentiate between metallic and non-metallic objects. The eddy current due to metal objects can be sensed by allowing a small signal through the charging pad. A wave-based detection requires an additional sensing device and a field-based detection method to sense the object by changes in an electric or magnetic field.

1) INFERENCES

The charging pads must be able to identify a vehicle that needs to be charged. A detecting circuit must deliver the signal to the inverter’s driving circuit. The adjacent charging stations should be detected by a detecting circuit installed in the vehicle. These operations must be synchronized with the speed of the vehicle. The additional detecting circuit is used to detect external living or metal objects.

- The controller unit drives the switches of the power inverter depending on the signal received from the detection circuits.
- The response of the detection circuit must be synchronized with the vehicle speed.
- A controller circuit must coordinate the vehicle and object detection sensor.

III. GRID-CONNECTED DYNAMIC WIRELESS CHARGING SYSTEM

The DWC system receives the power supply from a grid-tied power converter. The components of a grid-tied DWC system are a grid interface system with PFC, a bridge inverter, an impedance-matching network, charging couplers, and a diode rectifier on the vehicle side. Grid interfaces regulate power flow from the power grid to maintain d.c.-bus voltage. The d.c. voltage is converted into high-frequency a.c using a bridge inverter that energizes the receiver coil. This high-frequency a.c. power is converted to constant d.c.

by a diode rectifier to charge the EV batteries [65]. Generally, an effective grid-tied converter control strategy is vector control, which regulates the grid current using a rotating reference frame to individual active and reactive power. In this method, active and reactive power is indirectly controlled by tuning current controllers [65]. But, the DPC technique directly controls [66] the active and reactive power without depending on current regulators. This method directly identifies the voltage required by the converter within every switching period. A further benefit of this method is that it improves the dynamic response under fast power changes by controlling the converter voltage.

In the grid voltage synchronous dq reference frame, the equivalent circuit from the grid interface converter is shown in fig. 3. Grid voltage and current are defined as positive and negative sequences at the fundamental frequency due to the inherent imbalance of the distribution network. As a result, in the positive and negative synchronous reference frames, the grid-tied converter is expressed from (18) to (31) [65]

$$V_{grid\_dq+}^+ = L_{grid} \frac{di_{grid\_dq+}^+}{dt} + j\omega L_{grid} i_{grid\_dq+}^+ + V_{converter\_dq+}^+ \tag{18}$$

$$V_{grid\_dq-}^- = L_{grid} \frac{di_{grid\_dq-}^-}{dt} - j\omega L_{grid} i_{grid\_dq-}^- + V_{converter\_dq-}^- \tag{19}$$

Positive sequence components of grid voltage,

$$V_{grid\_dq+}^+ = V_{grid\_d+}^+ + jV_{grid\_q+}^+ \tag{20}$$

Positive sequence components of converter voltage,

$$V_{converter\_dq+}^+ = V_{converter\_d+}^+ + jV_{converter\_q+}^+ \tag{21}$$

Positive sequence components of grid current,

$$i_{grid\_dq+}^+ = i_{grid\_d+}^+ + ji_{grid\_q+}^+ \tag{22}$$

Negative sequence components of grid voltage,

$$V_{grid\_dq-}^- = V_{grid\_d-}^- + jV_{grid\_q-}^- \tag{23}$$

Negative sequence components of converter voltage,

$$V_{converter\_dq-}^- = V_{converter\_d-}^- + jV_{converter\_q-}^- \tag{24}$$

$$\begin{aligned} (1.5 \times \text{Re}(V_{converter} \times \hat{i}_{grid})) &= 1.5 \times \text{Re} \left\{ \left[ \left( \left( V_{grid\_dq+}^+ - L_{grid} \frac{di_{grid\_dq+}^+}{dt} - j\omega_1 L_{grid} i_{grid\_dq+}^+ \right) \times e^{j\omega_1 t} \right) \right. \right. \\ &\quad \left. \left. + \left( \left( V_{grid\_dq-}^- - L_{grid} \frac{di_{grid\_dq-}^-}{dt} - j\omega_1 L_{grid} i_{grid\_dq-}^- \right) \times e^{-j\omega_1 t} \right) \right] \right. \\ &\quad \left. \times \left( \left( i_{grid\_dq+}^+ \times e^{j\omega_1 t} \right) + \left( i_{grid\_dq-}^- \times e^{-j\omega_1 t} \right) \right) \right\} \tag{27} \end{aligned}$$

$$(1.5 \times \text{Re}(V_{converter} \times \hat{i}_{grid})) = P_{out0} + P_{outsin\_2nd} + P_{outcos\_2nd} \tag{28}$$

Negative sequence components of grid current,

$$i_{grid\_dq-}^- = i_{grid\_d-}^- + j i_{grid\_q-}^- \quad (25)$$

Grid-tied converters can be described by the power balance equation as follows

$$\left( C_{dc} \frac{dv_{dc}}{dt} \right) \times v_{dc} = \left( 1.5 \times \text{Re} \left( V_{converter} \times \hat{i}_{grid} \right) \right) - (i_{dc} \times v_{dc}) \quad (26)$$

where  $C_{dc}$ ,  $i_{dc}$ , and  $v_{dc}$  are d.c. link capacitors, d.c. side current, and d.c. side voltage respectively. In the grid-tied converter, an instantaneous active (real) power flow can be calculated by [65], as in (27) and (28), shown at the bottom of the previous page, where the average active (real) power can be represented as

$$P_{out0} = 1.5 \left[ \left( V_{grid\_d+}^+ \times i_{grid\_d+}^+ \right) + \left( V_{grid\_q+}^+ \times i_{grid\_q+}^+ \right) + \left( V_{grid\_d-}^- \times i_{grid\_d-}^- \right) + \left( V_{grid\_q-}^- \times i_{grid\_q-}^- \right) \right] \quad (29)$$

and the 2<sup>nd</sup> order of active (real) power ripples are expressed by

$$P_{outsin\_2nd} = 1.5 \left[ \left( V_{grid\_q-}^- \times i_{grid\_d+}^+ \right) - \left( V_{grid\_d-}^- \times i_{grid\_q+}^+ \right) - \left( V_{grid\_q+}^+ \times i_{grid\_d-}^- \right) + \left( V_{grid\_d+}^+ \times i_{grid\_q-}^- \right) \right] + 3\omega_1 L_{grid} \left( \left( i_{grid\_d+}^+ \times i_{grid\_d-}^- \right) + \left( i_{grid\_q+}^+ \times i_{grid\_q-}^- \right) \right) \quad (30)$$

$$P_{outcos\_2nd} = 1.5 \left[ \left( V_{grid\_d-}^- \times i_{grid\_d+}^+ \right) + \left( V_{grid\_q-}^- \times i_{grid\_q+}^+ \right) + \left( V_{grid\_d+}^+ \times i_{grid\_d-}^- \right) + \left( V_{grid\_q+}^+ \times i_{grid\_q-}^- \right) \right] + 3\omega_1 L_{grid} \left( \left( i_{grid\_q+}^+ \times i_{grid\_d-}^- \right) - \left( i_{grid\_d+}^+ \times i_{grid\_q-}^- \right) \right) \quad (31)$$

In the power equations (18) to (31), the 2<sup>nd</sup>-order active power ripples  $P_{outsin\_2nd}$  and  $P_{outcos\_2nd}$ , causing the d.c. voltage ripple will introduce the 2<sup>nd</sup> order power ripple in DWC output power. Furthermore, pulsating output power disturbs the d.c. bus voltage with large oscillations would further degrade the whole DWC system. Hence, to operate the DWC system without oscillations, the average output power and 2<sup>nd</sup>-order active power ripples should be regulated accurately and immediately. The proportional-integral-resonant controller is used to regulate the voltage, and the controller parameters are framed from the stochastic traffic model

(24h DWC system demand model) [67]. The model was developed with the help of the IEEE 13 bus distribution network.

The different scenarios [68] include sub-transmission based on the IEEE 9 bus system, distributed energy storage system connected to the distribution transformer's secondary side, and the d.c. Infrastructure through a solid-state power substation connected with the distribution transformer to maintain the voltage stability. The infrastructure cost of d.c. distribution is cheaper than energy storage but requires a flexible substation. The solar energy and electric storage system [69] is proposed to minimize the impact of the DWC system on the grid.

#### A. INFERENCES

Power quality difficulties such as voltage sag, harmonics, voltage and frequency instability, and EMI/EMC issues are among the hurdles in grid-connected WPT charging. The energy requirement of WPT charging stations should be considered while formulating the power flow diagram. The load changes of various charging system influence the dynamic responsiveness of the grid system. The energy demand of the grid system loses its stability due to the DWC system. It is difficult to forecast the energy requirements of various charging stations. During peak traffic on the roads, energy consumption is at its height. As a result, it is proposed that a local energy generating or storage facility be developed to deal with abrupt increases or decreases in energy demand.

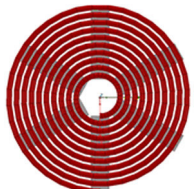
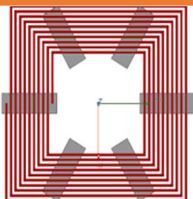
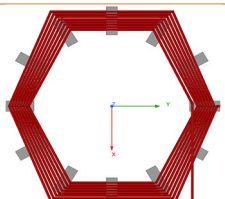
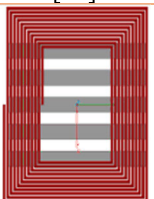
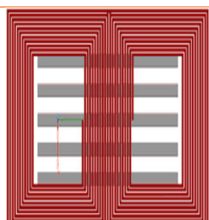
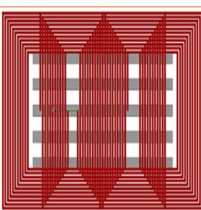
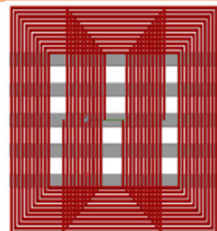
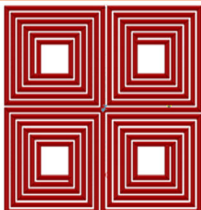
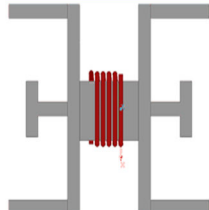

- The requirement of grid integration with WPT charging is power quality improvement, energy demand management, effective load forecasting, and a standalone energy source system.

#### IV. PV INTEGRATED DYNAMIC WIRELESS CHARGING SYSTEM

Evaluation in the EV market is depressed by the charging station. The utility grid will be affected if more charging stations are deployed. Hence, the energy demand will increase, resulting in more fossil fuel requirements. In recent years, the source of fossil fuels has been decaying. Also, the atmospheric temperature keeps on increasing. To avoid such issues, several countries aim to zero emissions by 2050. As a base, renewable energy-based power generation increased by 3% in the year 2020, which reduced the other fuels demand [70]. Also, the effect of decarbonization is accomplished by using renewable energy-based power generation. Such power generation has been booming in recent years in all sectors. The emission of greenhouse gases is reduced by PV-based sources. Hence, renewable energy-based EV charging will enhance road transport electrification. The PV-integrated DWC system is illustrated in Fig. 4. This scheme results in the growth of public charging stations, reducing the per unit energy consumption cost. It also reduces power integration and quality issues, saves costs with easy installation, and supports governing policy. A DWC system



TABLE 1. Different coil topologies.

Coil Type	Description	Coil Type	Description
 <p>Circular [43]</p>	<ul style="list-style-type: none"> <li>• The height of the vertical flux path generated by CP is 1/4<sup>th</sup> of the pad dimension.</li> <li>• Non-polarized pad and has a poor misalignment</li> <li>• Shielding impact is less</li> <li>• The simple system is used as a transmitter generally in SWC.</li> </ul>	 <p>Square [44]</p>	<ul style="list-style-type: none"> <li>• lower self-inductance than CP in fully aligned conditions.</li> <li>• The inductance value is increased due to sharp edges</li> <li>• Sharp edges generate eddy current and hot spots</li> <li>• Not suitable for high-power applications</li> </ul>
 <p>Hexagonal[45]</p>	<ul style="list-style-type: none"> <li>• At fully aligned, maximum power transfer efficiency</li> <li>• At misaligned, Poor power transfer efficiency</li> <li>• Non-polarized pad with low leakage flux</li> <li>• Commonly used on the receiver side</li> </ul>	 <p>Rectangular [23]</p>	<ul style="list-style-type: none"> <li>• Better than square and circular in horizontal misalignment.</li> <li>• The height of the vertical flux path generated by RP is 1/2<sup>th</sup> of the pad dimension</li> <li>• Non-polarized pad with moderate leakage flux</li> <li>• Commonly used in transmitter and receiver side</li> </ul>
 <p>Double D[23]</p>	<ul style="list-style-type: none"> <li>• Has a high shielding impact and a polarized pad.</li> <li>• Has lesser leakage flux</li> <li>• Commonly used on the transmitter side</li> <li>• It has greater horizontal misalignment tolerance than non-polarized pads</li> </ul>	 <p>Double D Quadrature[24]</p>	<ul style="list-style-type: none"> <li>• Better tolerance to horizontal and vertical misalignment</li> <li>• Requires two power converters to drive the DDQ pad</li> <li>• A better choice for the receiver side</li> <li>• Polarized pad with extremely low leakage flux</li> <li>• It provides a large charging zone</li> </ul>
 <p>Bipolar[25]</p>	<ul style="list-style-type: none"> <li>• Better tolerance to misalignment</li> <li>• Highly interoperable</li> <li>• Complex control strategy</li> <li>• Requires two power converters to drive the bipolar pad</li> <li>• The effect of k and shielding is high and commonly used on the transmitter and receiver side</li> </ul>	 <p>Quadrapule[48]</p>	<ul style="list-style-type: none"> <li>• Greater tolerance to misalignment</li> <li>• Polarized pad with lower leakage flux</li> <li>• Complex control strategy</li> <li>• Highly interoperable</li> <li>• Commonly used in transmitter and receiver side</li> </ul>
 <p>Flux pipe[24]</p>	<ul style="list-style-type: none"> <li>• Polarized pad with medium leakage flux</li> <li>• Provides a medium charging zone</li> <li>• Poor tolerance to misalignment</li> <li>• Poor interoperable</li> <li>• Commonly used in transmitter and receiver side</li> <li>• Higher impact of shielding</li> </ul>	 <p>Tripolar[49]</p>	<ul style="list-style-type: none"> <li>• Polarized pad with low leakage flux</li> <li>• Commonly used in transmitter and receiver side</li> <li>• It provides a large charging zone</li> <li>• Highly interoperable</li> <li>• Greater tolerance to misalignment</li> <li>• Poor impact of shielding</li> </ul>

is upgraded to a green transportation system by integrating renewable energy sources. E-bike charging stations [71] and road surveillance systems [72] with solar panels promote green transportation. Solar energy is abundant along the long national highways. Along the roadside, solar energy can be extracted to the maximum extent. Solar panels are installed along many countries' roadsides to generate power, which

is transferred through long transmission lines to users [73]. France develops the first solar road measuring 1 km and 2800 m<sup>2</sup> [74]. This solar energy might be used to operate the DWC system and to improve the dynamic response of the grid-tied DWC system [75]. A demand-side management algorithm is proposed to decrease the carbon footprint generated by road transportation. The developed methodology

TABLE 2. Different compensation topologies.

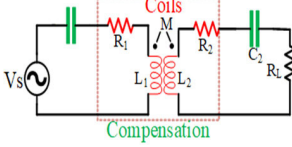
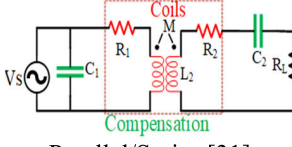
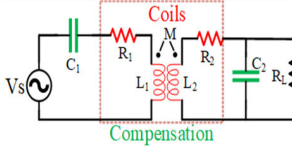
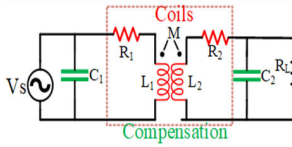
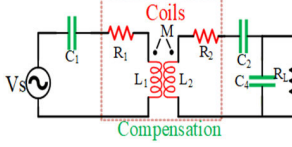
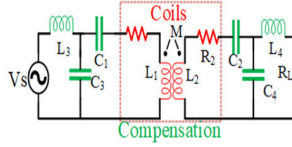
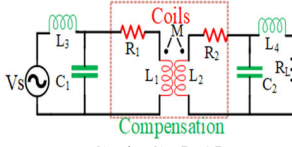
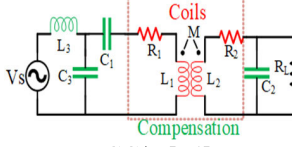
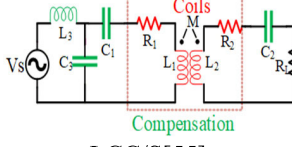
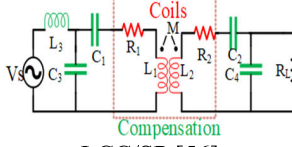
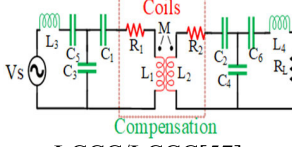
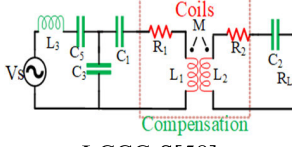
Compensation Type	Description	Compensation Type	Description
 <p>Series/Series [50][46][47]</p>	<ul style="list-style-type: none"> <li>• Output current is independent of load and resonant frequency</li> <li>• Better efficiency than series/parallel</li> <li>• Required low d.c.-link voltage</li> <li>• HF series capacitor current leads to getting high capacitor voltage</li> </ul>	 <p>Parallel/Series [31]</p>	<ul style="list-style-type: none"> <li>• Higher voltage is required than series/series and series/parallel</li> <li>• Total impedance increases with misalignment</li> <li>• Requires input current source and significant input resistance</li> </ul>
 <p>Series/Parallel[31]</p>	<ul style="list-style-type: none"> <li>• Required low d.c.-link voltage</li> <li>• Total impedance decreased with misalignment</li> <li>• Receiver coil self-inductance must be smaller than series/series</li> </ul>	 <p>Parallel/Parallel [33]</p>	<ul style="list-style-type: none"> <li>• Total impedance increases with misalignment</li> <li>• Dependent on coupling co-efficient and load resistance</li> <li>• Requires high input current source and considerable input resistance</li> </ul>
 <p>Series/Series-Parallel[51]</p>	<ul style="list-style-type: none"> <li>• Load change and co-efficient of coupling do not affect the gain value</li> <li>• In wider parameter variations, circulating losses are low</li> <li>• It can be used in a wide range of parameters</li> </ul>	 <p>LCC/LCC[52]</p>	<ul style="list-style-type: none"> <li>• Possible to achieve zero current switching</li> <li>• Electrical characteristics can be affected by the inductance parameters</li> <li>• Lesser sensitive to the inductance variations</li> </ul>
 <p>LCL/LCL[53]</p>	<ul style="list-style-type: none"> <li>• Providing active power to the load is sufficient for the inverter</li> <li>• Transmitter-coil current is independent of load condition</li> <li>• Weak ability to suppress higher-order harmonics</li> </ul>	 <p>LCC/P [54]</p>	<ul style="list-style-type: none"> <li>• Has a more compact receiver than LCC/LCC</li> <li>• Higher efficiency than series/series</li> <li>• Smaller conduction losses of the inverter</li> </ul>
 <p>LCC/S[55]</p>	<ul style="list-style-type: none"> <li>• Higher design freedom</li> <li>• Achieved constant output current</li> <li>• Simple ZVS achievement</li> <li>• No control circuit required</li> </ul>	 <p>LCC/SP [56]</p>	<ul style="list-style-type: none"> <li>• High misalignment tolerance</li> <li>• Achievable ZVS operation</li> <li>• Higher design freedom</li> <li>• Smoothing the transmission power fluctuation</li> </ul>
 <p>LCCC/LCCC[57]</p>	<ul style="list-style-type: none"> <li>• Fast and accurate tuning technique</li> <li>• Can avoid burning of power supply due to compensation network by tuned passive elements</li> <li>• Suitable for a stable and efficient charging system</li> </ul>	 <p>LCCC-S[58]</p>	<ul style="list-style-type: none"> <li>• At two separate ZPA frequency points enables CC and CV modes</li> <li>• The receiver side is lighter and more compact</li> </ul>

TABLE 3. Different primary side converter topologies.

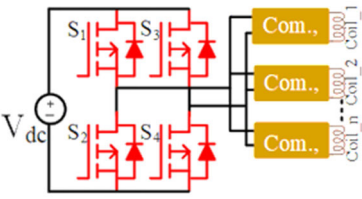
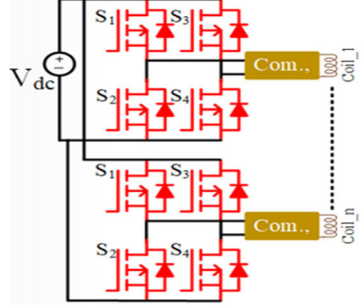
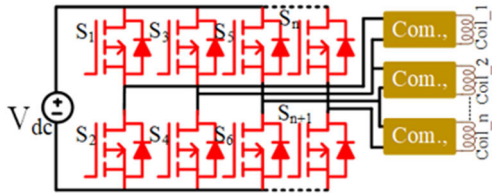
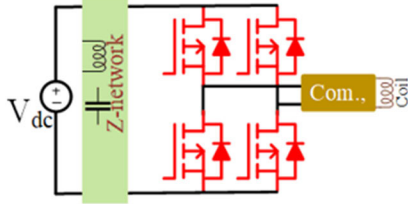
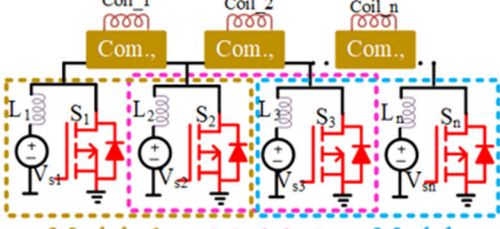
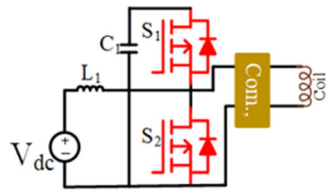
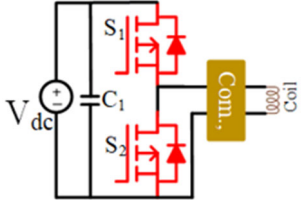
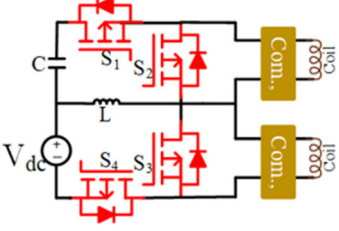
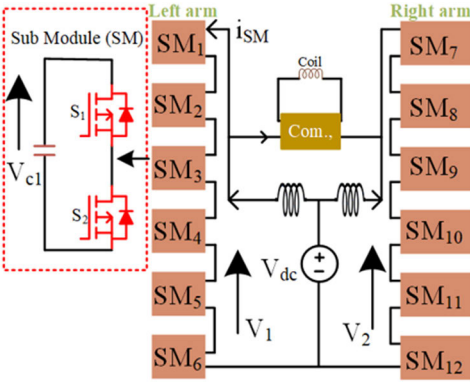
Inverter topology	Description
 <p>Two-legged inverter N coils[36]</p>	<ul style="list-style-type: none"> <li>• It is more suitable for SWC due to its low reliability and constrained power level.</li> <li>• More adoptable as a multi-output charger</li> <li>• Provides sufficient space for installation</li> <li>• The number of switches required to drive the N number of coils is 4</li> <li>• Due to poor efficiency not suitable for DWC</li> <li>• High power loss due to current flow in non-interactive charging couplers</li> </ul>
 <p>N two-legged inverter N coils[39]</p>	<ul style="list-style-type: none"> <li>• Delivering constant power to all the coils</li> <li>• Effectively driving the segmented coils</li> <li>• Suitable for monorail and DWC system</li> <li>• The number of switches required to drive the N number of coils is 4N</li> <li>• High initial cost due to the high number of switches</li> <li>• The system becomes heavier due to a more significant number of switches</li> </ul>
 <p>N-legged inverter N-1 coils [12] [13]</p>	<ul style="list-style-type: none"> <li>• Transmitter coils are energized smoothly</li> <li>• Minimum current flow in non-interactive charging couplers</li> <li>• Only one additional leg is required</li> <li>• The number of switches required to drive the N number of coils is 2(N+1)</li> <li>• Effective driving pulses are required to drive the charging coupler</li> </ul>
 <p>N Z source inverter N coils[59]</p>	<ul style="list-style-type: none"> <li>• No additional circuitry or semiconductors are necessary to automatically correct the power factor and regulate the system output voltage</li> <li>• As a result, it is suitable for applications requiring high power since it is insensitive to shoot-through states, making it more reliable</li> </ul>
 <p>An inductive coupler array[60]</p>	<ul style="list-style-type: none"> <li>• Push-pull driven coupler array is proposed to reduce the number of switches required to drive the charging couplers</li> <li>• The number of switches required to drive the N number of coils is (N+1)</li> <li>• Constraint to high power level due to the limited power rating of the semiconductor switches</li> <li>• The current stress on the switches doesn't increase</li> </ul>
 <p>Active clamping half-bridge boost inverter[61]</p>	<ul style="list-style-type: none"> <li>• The fixed frequency control method</li> <li>• ZVS is possible</li> <li>• Reducing the switching losses</li> <li>• Bifurcation can be avoidable</li> <li>• Can regulate the charging current with a quick response</li> </ul>

TABLE 3. (Continued.) Different primary side converter topologies.

 <p>Class D Half bridge inverter[62]</p>	<ul style="list-style-type: none"> <li>• Achieved ZVS effectively when the output impedance angle of the inverter is higher than 0</li> <li>• The operating frequency of the inverter is properly regulated</li> <li>• Achieving good dynamic response</li> <li>• More suitable for the SWC system</li> </ul>
 <p>Dual independent output inverter[63]</p>	<ul style="list-style-type: none"> <li>• By allowing the device to drive two transmitter coils independently, two independent outputs can be produced, and four output states can be operated simultaneously.</li> <li>• Lesser number of power switches than conventional inverters</li> <li>• Higher redundancy than multi-output chargers</li> <li>• Simple design</li> </ul>
 <p>Integrated boost multilevel inverter[64]</p>	<ul style="list-style-type: none"> <li>• High voltage stress is shared by a large number of low voltage switches</li> <li>• The heatsink of the small size required</li> <li>• Low switching losses result in higher efficiency</li> </ul>

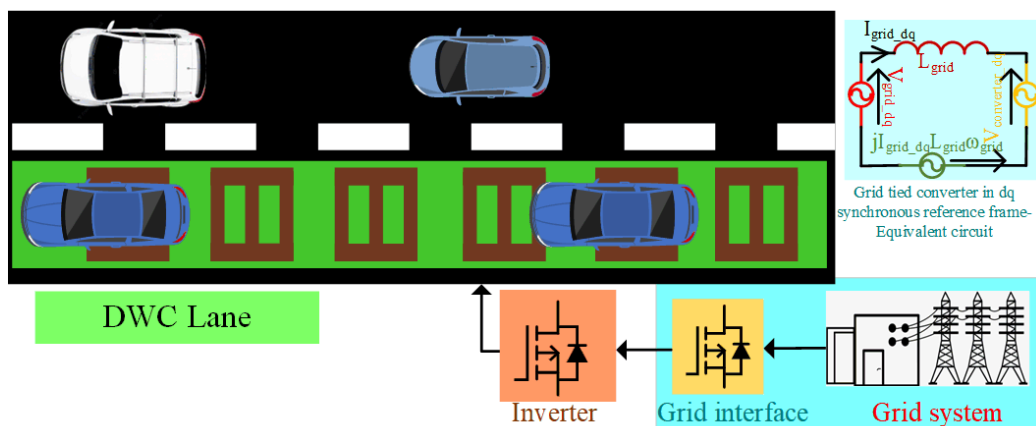


FIGURE 3. Grid-tied DWC System.

considered the optimized algorithm smoothens the power demand profile by reducing the energy drawn from the grid, improving system fairness, and reducing carbon emissions by 22% through local renewable energy generation. The power demand profile of the DWC system is smoothly maintained

by integrating wind energy [76] with the grid system. When the wind energy system satisfies the requirement of DWC demand, the power demand satisfied by the grid becomes zero. The wind energy system assists the grid system in maintaining the smooth load curve by assisting in the peak



demand period. The wind, solar, and energy storage system are integrated with the DWC system [77], and the optimized algorithm was developed to maintain the smooth load profile at peak demand periods. The developed algorithm reduces the operational cost of the DWC system by decreasing the impact of the grid on the DWC system.

#### A. INFERENCES

The PV-integrated grid-tied WPT technology helps the grid system to maintain a consistent voltage profile and power flow. Peak demand for the grid system may be fulfilled by solar electricity produced at that time.

The optimized algorithms are used to smoothen the demand profile of the PV-integrated grid-tied WPT charging system. This renewable energy integration may lower the charging system's energy consumption cost.

- Weather forecasting is necessary to satisfy the energy deficit of the grid system during peak hours.
- An additional storage set-up is required in the absence of renewable sources.
- Power system planning is a prerequisite of the renewable integrated grid-connected WPT system.

#### V. DESIGN AND CHALLENGES OF THE DWC SYSTEM

In a DWC system, the main objective of the DWC system is that the power delivered by the charging system should be greater than the battery power taken by the vehicle to cover the entire track. And also, the impact of the DWC system on a grid side and the energization of transmitter coils concerning vehicle speed are complex parameters that a proper design process can overcome. The vehicle should be charged within a specified time. The charging period is similar to a transient condition. The longitudinal and lateral misalignment tolerance will affect the power transfer in the vehicle's movement. The misalignment tolerance level is improved by designing a proper coil structure and impedance-matching network. The positioned coil should be interoperable. So, the system will be effective irrespective of the vehicle's coil symmetry and charging power levels. The design of the system should be adaptable to international standards. The initial infrastructure cost decides the implementation of the system on the roadside. The economics of the system will be analyzed based on the number of DWC charging vehicles utilizing the roadways. The cost will be reduced when the number of users utilizing the road is increased. Fig. 5. addresses the objectives of the various parameters in the DWC system. An increase the vehicle usage on the track will decrease the volume of the battery. The life span of the system will be considered based on the location of the system and environmental factors. A dynamic charging system also improves the efficiency and life span of the battery. The different topologies and sectors are involved in designing the DWC system. The step-by-step design process is represented in fig. 6. The first stage of the DWC system is deciding the power level. The transmitter and receiver coil should be designed according to that power level. Then, the impedance matching network is considered

based on coil parameters. The resonant network is designed to resonate based on the inductance of the charging pads. This will help the system achieve frequency tolerance and maximum power transfer. Then, the power converters will be designed based on coil and compensation networks. The power converter switches must withstand the operating power and frequency. The driver unit of the power converters should generate signals for power switches with vehicle position or coil alignment concerns. The identification of foreign objects is mandatory to avoid the unwanted temperature rise in the charging system.

The energization and de-energization of the coil are controlled by the power inverter. The power inverter is generated the control signal based on the signal acquired from the detection circuit. The system will operate depending on the signal acquired from the vehicle identification unit. The power transfer frequency and magnetic and electric field strength around the coil should be unharmed to living objects. This could be possible by providing proper aluminum shielding. Additional efforts are required beyond the WPT3 level. Finally, all the designed parameters strictly adapt to the international standards developed by mobility organizations

#### VI. DIFFERENT CASE STUDIES

##### A. 50 kW SYSTEM

Various organizations are developed a 50-kW inductive power transfer charging system [78], [79]. A researcher, Roman boss demanding from SFIT, Zurich, developed a 50-kW charging pad [79] and analyzed the different charging pad structures [80] and semiconductor switches [81]. Varghese, Benny et al. [82] developed modified coils embedded in the concrete structure for dynamic charging. The researchers from ORNL developed a 3  $\Phi$ , 50 kW charging system with a bipolar structure [83]. Then the modified 3  $\Phi$ , LCC-LCC compensation method was discussed by ORNL with Non-Zero coupling in the interphase system [84]. Additionally, the researchers allowed 22 kHz and 85 kHz frequencies in a 50-kW system and analyzed them [78]. The proper shield for a 50-kW system was designed and analyzed by ORNL [85]. The Zhejiang University researcher proposed [86] a three-channel charging system to reduce the stray magnetic field like a DD pad. A researcher, Roman boss hard, developed a 50-kW rectangular pad and analyzed the advantages of that pad over the DD pad. The charging pad was energized by a full-bridge ZVS inverter. A single switch in a full-bridge inverter is formed by three parallelly connected SiC C2M0025120D (1200 V/ 0.025  $\Omega$ ) MOSFET to handle the high RMS current (120 A). The same configuration of SiC MOSFET is used in the receiver-side synchronous rectifier.

The efficiency achieved by the developed rectangular charging pad system is 95,8% at a 16 cm gap on Z-axis and 92% at a 15 cm gap. The system achieved 96.16% peak efficiency at 33,2 kW power. The mentioned efficiency is based on d.c.- d.c. conversion stages. The dimension of the charging pad is 630\*400\*50 mm<sup>3</sup> ( $L_{coil}^*$   $W_{coil}^*$   $W_{cu}$ ). The Litz

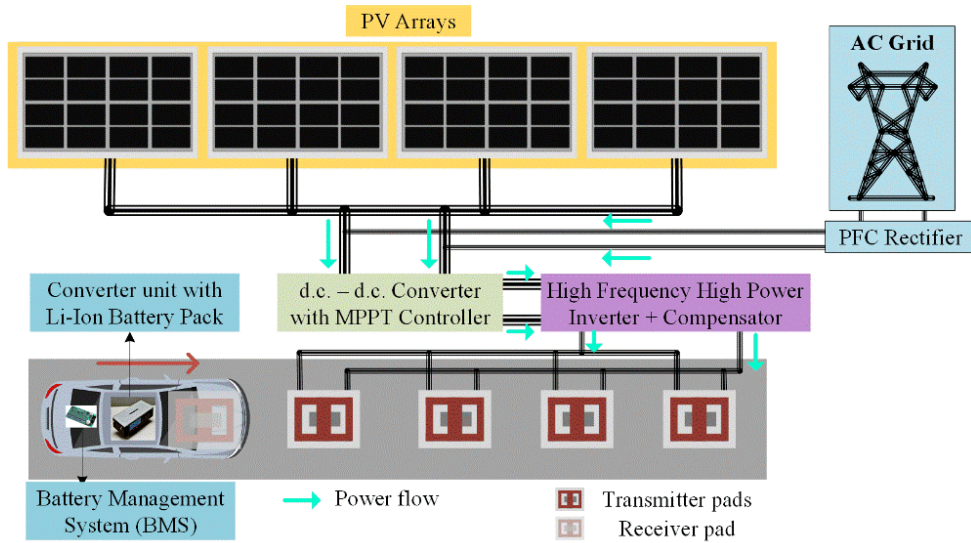


FIGURE 4. PV integrated DWC system.

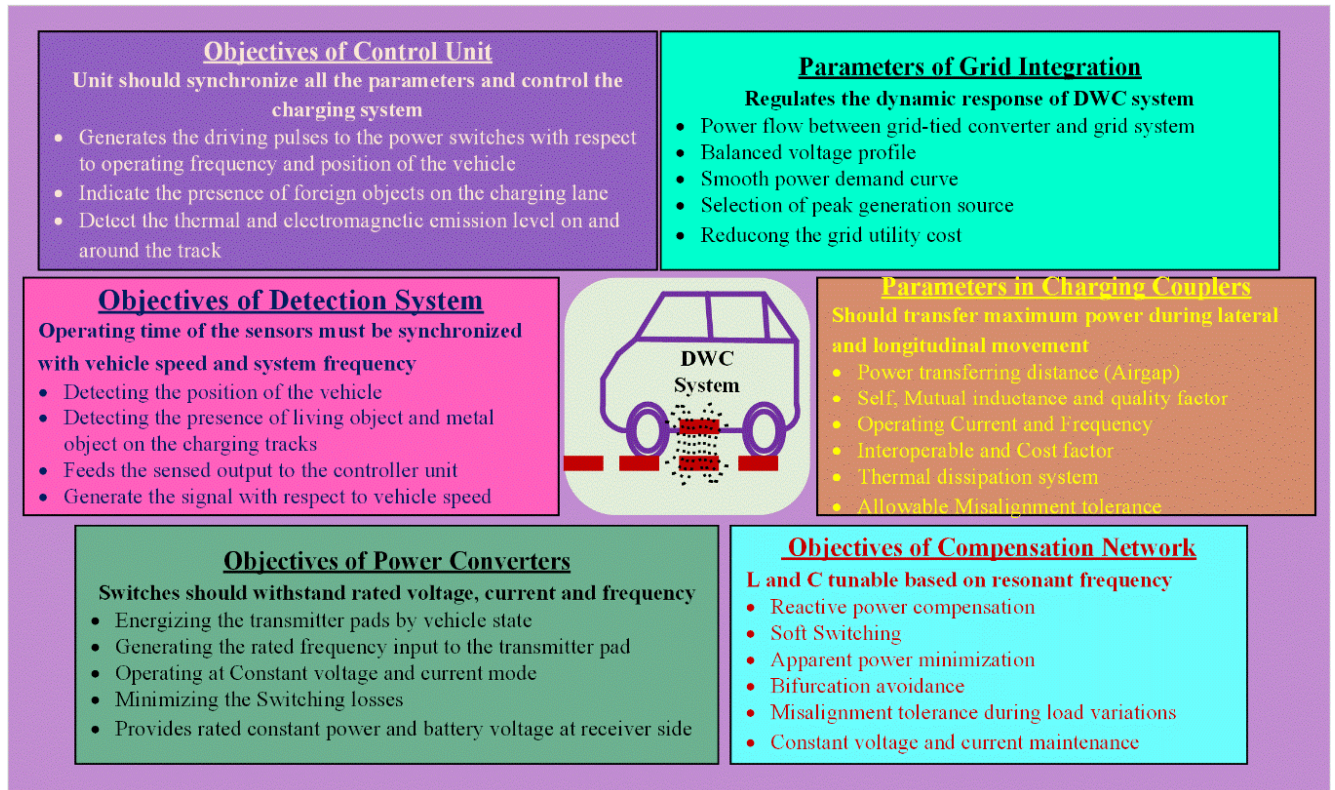


FIGURE 5. Objectives and parameters of DWC components.

wire with 2500 strands is used to design the coil with a 7.4 mm outer diameter, and the diameter of the individual strand is 0.1 mm. The manganese-zinc power ferrite K2004 is used as a core to distribute the uniform flux. The 2 mm thickness of oxygen-free copper shields the magnetic field emission. The series-series compensation is used due to the symmetric

topology of charging pads, and the circulating VAR through the charging pads is low with light load conditions.

A charging pad structure and converter topology of the 50-kW charging system are mentioned in fig. 7. In the compensation, CSP 120-200 polypropylene film capacitors with forced-air cooling (aluminum heat sink mounted on



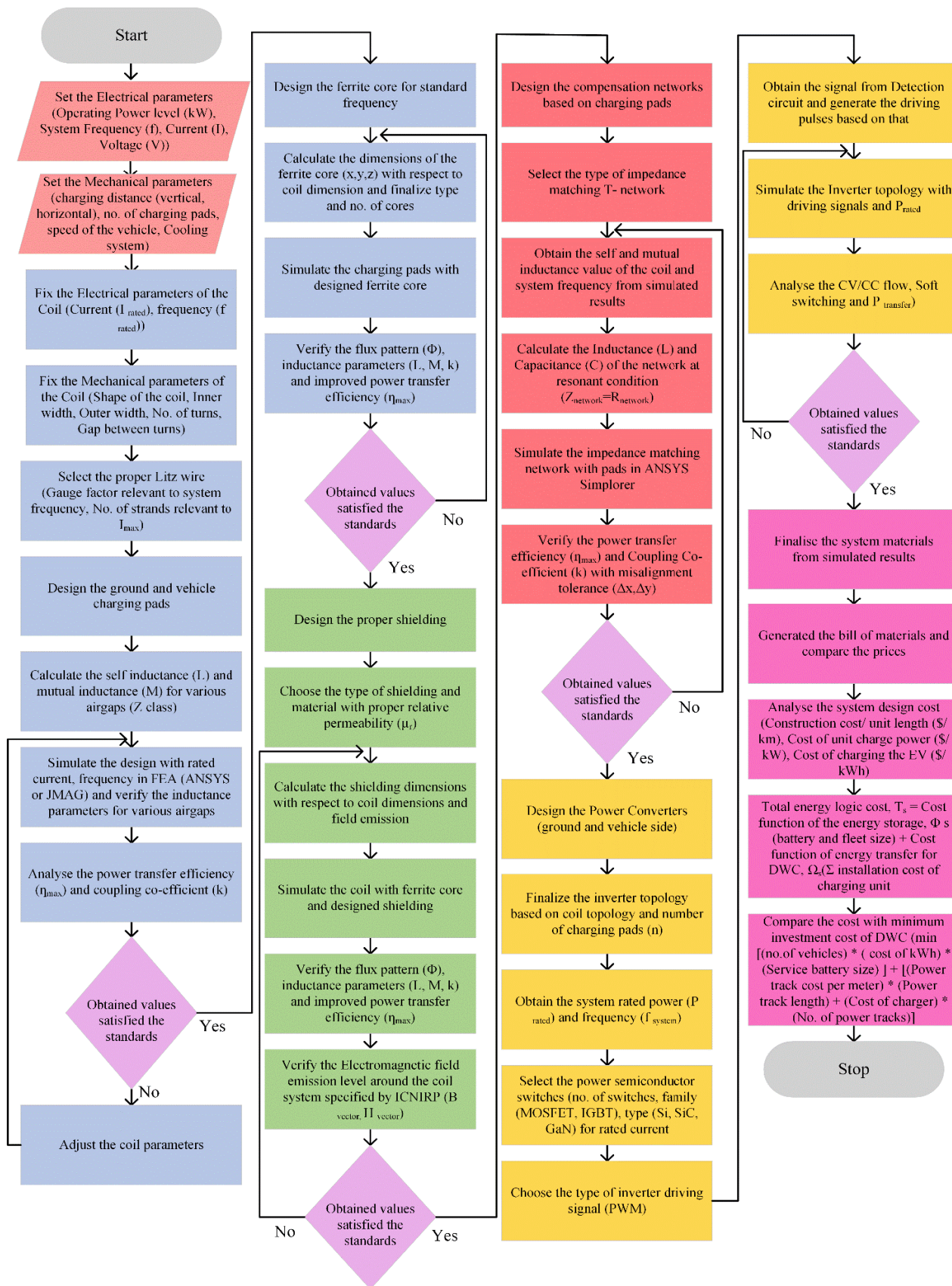


FIGURE 6. Design flow chart of DWC components.

the capacitor) are used in this system. Thermocouples measure the temperature of the system. The designed system parameters are mentioned in Table 4. A researcher compared the performance of the designed rectangular pad with the DD-pad [80] and ABB Switzerland supports the work. A group of researchers from Utah University [82] investigated the mechanical features of concrete pavements and the effect of ferrite spacing on losses in a 50-kW dynamic charging system. Providing optimal spacing and using fiber-class rebar in a concrete structure will improve efficiency. The 50-kW rectangular and double D-pad charging structure was analyzed by [80] and represented in Table 5. Ibrahim from Zhejiang University developed a 50 kW three-channel inductive charging system to chase the advantages of the proposed structure [79], [86]. The three-channel structure decreases the cross-coupling effect of the adjacent charging pads and reduces the effect of the stray magnetic field. The achieved stray magnetic field of the proposed structure is  $4.8 \mu\text{T}$ , where  $13 \mu\text{T}$  for the DD pad and  $24 \mu\text{T}$  for the rectangular pad. The proposed asymmetric three-channel structure with optimal power distribution of 20:60:20 reduces the stray magnetic field by 63% of the DD pad and 80% of the rectangular pad. The achieved stray magnetic field reduction is 58% of the rectangular pad and 23 % of the DD pad by utilizing average power distribution. The stray magnetic fields can be reduced by using three pad structure. (Table 6.)

TABLE 4. Parameters of 50 kW system [83].

Parameter	Variable	Value
Length of the coil	$L_{\text{coil}}$	63 cm
Width of the coil	$W_{\text{coil}}$	38 cm
Width of the winding	$w_{\text{cu}}$	6.75 cm
Position of the winding	$d_{\text{cu}}$	12.5 cm
No. of I-type cores (I-126/20, K2004)		5
No. of turns	$N_1, N_2$	9.5
Transmitter and Receiver coil Self-Inductance	$L_1, L_2$	71.6 $\mu\text{H}$
Mutual Inductance of the coils	$M$	16.5 $\mu\text{H}$
Coupling Coefficient	$k$	0.2299
Compensation capacitor (CSP 120-200)	$C_1, C_2$	0.0541 $\mu\text{F}$
d.c.-Link voltage of the transmitter	$V_1$	800 V
d.c.-Link voltage of the receiver	$V_2$	800 V
Required Battery voltage	$V_{\text{batt}}$	600 V
RMS value of transmitter current	$I_1$	87.3 A
RMS value of receiver's current	$I_2$	69.7 A
Airgap (Z class)	$Z_{\text{Ideal}}/Z_{\text{Worst}}$	16/15 cm
Transmitting power frequency	$f_0$	85 kHz
Litz wire strands	2500 * 0.1 mm	
Shielding (oxygen-free copper)	210*280 $\text{m}^2$ & 2mm thick	
Rating of power electronic switch TO-247	C2M0025120D	1200 V
	$R_{\text{on}} = 25 \text{ m}\Omega$	
Coil housing	410 * 760 * 60 $\text{mm}^3$	
Losses (Transmitter/Receiver)	764.9W/543.4W	

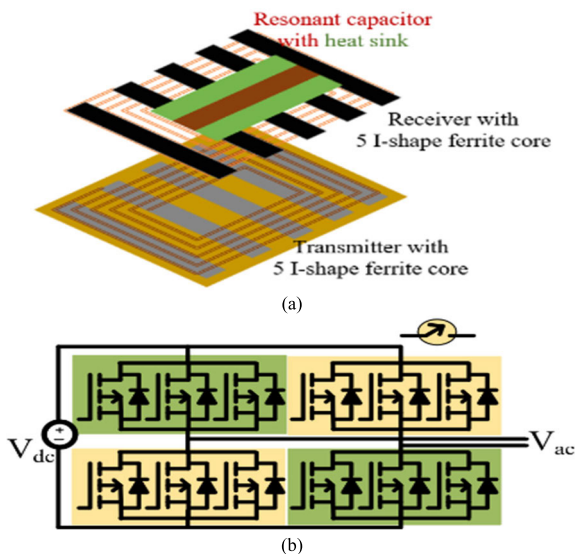


FIGURE 7. 50-kW IPT charging system (a) coil shape and (b) power inverter.

**B. 11 kW SYSTEM**

A Researcher from SAE developed an 11-kW bench test set up with DD coil structures [87]. The efficiency achieved by the designed coil is  $>85\%$  in aligned conditions and  $>80\%$  in misaligned conditions. The test results are performed in  $>0.96$  power factor. The strength level of the magnetic field throughout the test is less than 21 A/m, and the electric field

is 80 V/m. The receiver charging pad, ferrite, compensation circuits, rectifier unit, aluminum shielding, and a standardized steel mimic plate are placed inside a strut frame made of fiberglass.

The effect of heating should be considered while designing the systems. The interoperable performance of the DD pad was also analyzed by using a different power level of vehicle assemblies. The azimuth pattern represents the emission level of the charging pads in various misalignment conditions. A [56] and [88] 11-kW charging system with an asymmetric DD coupler was implemented with different

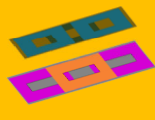
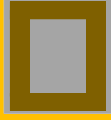



**TABLE 5. Comparative evaluation of DD and rectangular pad [80].**

Rectangular pad	DD- Pad
High transmission efficiency	The transmission efficiency of the DD pad is lower than the rectangular pad for the same outer dimensions by 0.5%
For the same gravimetric power density, a highly efficient design	For the same gravimetric power density, 1% points less efficient design than rectangular winding
Poor degree of freedom for magnetic coupling due to low $w_{cu}$	The high degree of freedom for magnetic coupling due to large $w_{cu}$
Low core flux density	High core flux density
The required core material is low	The required core material is high
High magnetic stray field	Reduced magnetic stray field by the factor 2 than rectangular pad
The area required, and mass of the coil are low	The area required, and mass of the coil are high
High shielding loss	Low shielding loss
Low ferrite and copper loss	High ferrite and copper loss
Suitable for light-weight on-board chargers	Suitable for short-distance stray magnetic field standards and satisfactory conditions

control topologies represented in fig. 8. In [56] and [88], the LCC-SP compensation network with a secondary side current doubler was developed. A developed system achieved 91.286% of efficiency at the maximum offset condition in the horizontal direction. A researcher at Tongji University developed this system to improve power transmission efficiency by VAR compensation. The developed LCC-SP topology has a high degree of freedom, reduced complex design of secondary, reduction of higher-order harmonics, and soft switching can be achieved. The current doubler rectifier is integrated with the receiver side to overcome the restriction of limited battery voltage. The designer should consider the effect of higher-order harmonics increasing the turn-off current. A researcher from TU delft [89] analyzed and optimized an 11-kW dynamic charging system. He proposed a multi-objective optimization method to determine the Pareto front of the double D-pad. The efficiency of the optimized system is 96.82%. The SS compensation is used to compensate the VAR. The Agilent 4294A impedance analyzer measured the parameters of the magnetic components. The estimated tolerance of L is 1%, and M is 3%. An 11-kW integrated boost interleaved multi-level converter with LCC compensation was developed by Auckland university [90]. An 11-kW charging system with a secondary side current doubler is mentioned in fig.8c.

**TABLE 6. Reduction of a stray magnetic field by 3 coil pads with different power distributions [89], [90].**

			
Transmitter & receiver	Three coil asymmetric pads	Symmetric rectangular	Symmetric DD
Stray magnetic field	4.8 $\mu$ T in 2:6:2 power distribution	24 $\mu$ T	13 $\mu$ T
	10 $\mu$ T for average power distribution		

**TABLE 7. Optimized parameters of 11 kW system [89].**

Parameter	Variable	Value
SiC MOSFET TO247-3	C2M0040120D	1200 V, 55 A, 40 m $\Omega$
SiC Schottky diodes TO247-3	C4D40120D	1200 V, 54 A
Power ferrites	TDK N87	Mn-Zn, $\mu_r=2200$
Number of ferrites	5/3 (117 mm*15.8 mm*34 mm)	
Litz Wire	4.8 mm * 525 (AWG 41)	
Primary Coil	DD (inner length)	31.9 mm
	DD (inner width)	25 mm
Secondary Coil	DD (inner length)	28 mm
	DD (inner width)	13.3 mm
transmission efficiency (%)	d.c.-d.c., $\eta$	96.92

Table 7 and Table 8 represent optimized parameters of an 11-kW system developed by different researchers.

**C. 20 kW AND 25 kW SYSTEM**

In [92], Utah State University developed a 25-kW dynamic charging system for the bus with a 35 cm circular pad. Additionally, they developed the system with the vehicle detection system. The dual loop controller (current controller and power controller) is integrated into the primary converter side to regulate the current and power within the permissible limit. The generalized state-space averaging method is used to design the dual loop controller. The purpose of the dual-loop controller is to provide a good dynamic response while regulating the primary side current and energizing the primary pads effectively. In the EV detection system

TABLE 8. Parameters of 11 kW system [88], [91].

Parameter	Variable	Value
Processor	TMS320F28335	DSP
SiC MOSFET TO247-3	IMW120R045M1	45 mΩ, 1200 V, I <sub>D</sub> = 52A
Schottky diodes TO247-2LD	FFSH30120A	1200 V, 46 A
Power ferrites	TDK PC95	Mn-Zn, u <sub>r</sub> =3300
Litz Wire	5 mm * 1300 strands	
Primary Coil	DD	544 mm*574 mm
Secondary Coil	DD	420 mm*260 mm
Airgap	150 mm	
Power	11.044 kW	
Battery Voltage	V <sub>b</sub>	400 V
Charging Current	I <sub>b</sub>	27,522 A
Input d.c. voltage	V <sub>in</sub>	800 V
Input d.c.	I <sub>in rms</sub>	16.294 A
transmission efficiency (%)	d.c.-d.c., η	91.870

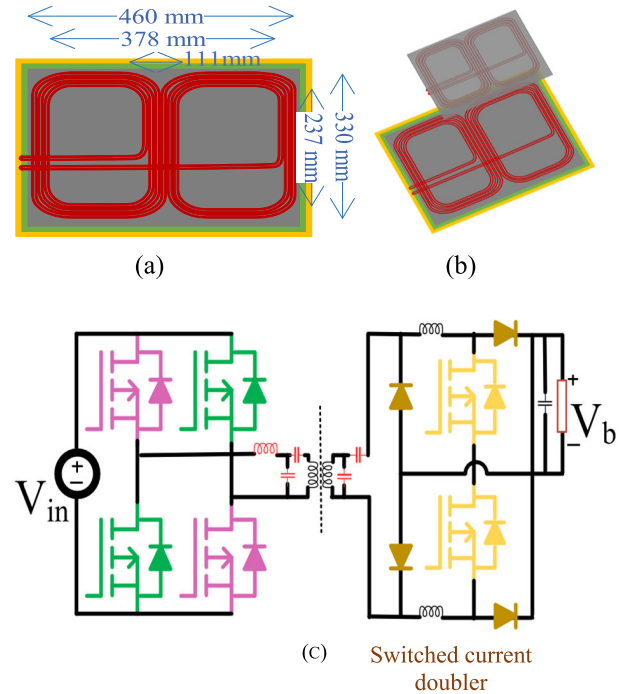


FIGURE 8. 11-kW IPT charging system (a) DD coil shape by SAE (b) asymmetric DD pad (c) LCC-SP topology with switching current doubler [88], [91].

$$\begin{aligned} &\text{Weighted touch current (perception/ reaction)} \\ &= \frac{U_2}{500} \end{aligned} \quad (32)$$

single primary coil is positioned under the vehicle, and three secondary coils are placed in front of the primary charging track. The operating voltage level of the detection system is 0-5.1 V. The reference value of the primary current is maintained within 75 A by the current controller, and the battery charging power is limited to 20 kW by the power controller. The track is developed with two circular charging pads. One pad is mounted within fiberglass grates, and another within a concrete structure. The achieved energy efficiency of the developed system is 86%, and the power efficiency is around 90%. Reference [93] developed a testing model for EMF and the effect of touch currents on the living object from a 25-kW dynamic charging system on the NREL campus. The charging system is used to power the shuttle on the NREL campus. The charging pad structure of the 20 kHz, 25-kW wireless charger is symmetrical and square with 35 inch<sup>2</sup>.

The S-S topology is used in the compensation segment. The radio frequency and low-power excitation systems are integrated into the system, which assists the automatic vehicle alignment with pad structures. The safe perimeter boundary is set by 4 feet around the shuttle. A 25-kW system with a primary side controller is represented in fig. 9a.

$$\begin{aligned} R_s &= 1500\Omega, \quad R_1 = 10000\Omega, \quad R_B = 500\Omega, \\ C_1 &= 0.022\mu F, \quad C_s = 0.22\mu F \end{aligned}$$

The peak value of weighted touch current can be determined by (32). An EMF is measured using a probe analyzer with a low-frequency isotropic field (EHP-50D 5 Hz-100 kHz). The EMF level could be measured and limited based on IEEE C.95.1, ICNIRP 2010, IEC 61980-3, and ACGIH TLV 2017. Leakage current tester TOS3200 measures the touch current. The circuit represented in fig. 9b. is developed by IS/IEC standards and used to measure the touch current [94]. The measured data from the different misalignment conditions was used to analyze the exposure level. As per ICNIRP, the nominal touch current is 5.66 mA at 20 kHz. The measured touch current value between the vehicle door and ground is 5.943 mA at an operating frequency of 21 kHz. Delft university [95] designed a 20-kW dynamic charging system and optimized the selection of pad structures and compensation networks. The optimization procedure suggests that the S-S topology and rectangular pad are more suitable for this 20-kW design. The P compensation on the secondary side is not valuable where the misalignment tolerance is considered. The series of LCC compensation is favorable on the receiver side due to reduced size and improved power transfer efficiency. On the primary side, the same types of compensations are also satisfactory due to having ZPA and the reduced power requirement of power switches. The efficiency of the S-S compensation is higher

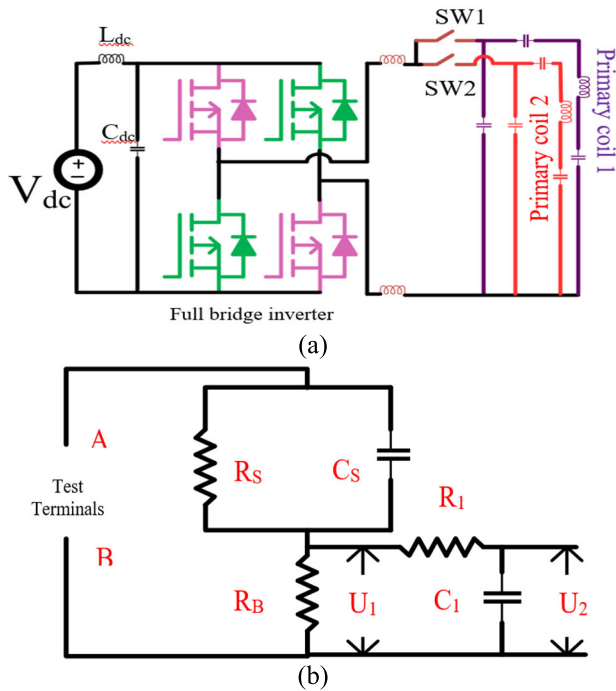


**FIGURE 9.** (a) 25-kW IPT charging system with primary-side controller [82] (b) Measuring network, weighted touch current (perception or reaction) [96].

than the D-LCC compensation at the same level of mutual inductance and output power. The power transfer capability on the secondary side of the system can be maximized by  $\Phi_{12} = \pi/2$ .

The size of the receiver pad might be small compared with the transmitter pad at a high-power level due to vehicle size constraints. The power transfer efficiency of the rectangular pad is higher than the other polarized and non-polarized pads. An ORNL researcher [85] developed a stationary wireless charging system for Toyota RAV4 electric vehicles. The symmetrical coil transferred a 22 kHz, 20 kW power with nominal coupling co-efficient of 0.265- and 162-mm airgap. The d.c. input parameters of the designed system are 424 V, 83.16 A, and the output parameters of the designed inverter are 384 V, 58.27 A. The inverter is developed by using 600 V/ 600 A Powerex PM600DV1A060 IGBT modules. The d.c.- d.c. the efficiency of the system is 95.037%. Table 9 represents the optimized parameters of the 20-kW system developed by a researcher.

**D. 7.7 kW SYSTEM**

A researcher Weihan Li from Hefei University has worked with other researchers and developed a 7.7 kW charging system. The feasibility of the charging system [25], [97] is analyzed and a bipolar coil is developed. The S-S compensation is compared with LCC compensation and the LCC compensation network is suggested for high misalignment tolerance conditions [98]. The LCL network assists the inverter to supply the active power required by the load at the resonant

**TABLE 9.** Optimized parameters of 20 kW system [95].

Parameter	Variable	Value
Output Power	$P_{out}$	20 kW
Airgap Distance	$Z$	150 mm
Operating frequency	$f$	85 kHz
d.c. voltage limit	$V_{dc, max}$	850
Lateral misalignment	$\Delta x$	150 mm
Number of turns	$N_1/N_2$	23/31
Number of ferrites	$N_{fe}$	7/5
Ferrite dimensions	$T_x$ side	515.3*27.7*28.8 mm
Ferrite dimensions	$R_x$ side	243.1*27.7*28.8 mm
The distance between each ferrite		41.8 mm/69.3 mm
The distance between coil & ferrite		3.9mm /1 mm
The distance between the shield & ferrite		10.6 mm/15 mm
Inner length of the pads	$L_{in}$	184.7 mm/66.2 mm
The inner width of the pads	$W_{in}$	220.8 mm/114.2 mm
Distance between pad turns		2.2 mm
Transmitter and receiver pad		Rectangular
SiC MOSFET,		1200 V, 56 A, 30 mΩ, PG-IMZ120R030M1H
d.c. Source		CINERGIA GE20 (0-750) V
Efficiency at fully aligned		97.2%
Efficiency at misaligned		94.1%

condition and makes the transmitter current independent of load. The features of S-S topology and double-sided LCC topology are specified in Table 11. The LCC network is used to perform the switching operation in zero current modes by tuning the compensation circuit parameters and ensuring the unity power factor pick-up on the receiver side [52]. The 600 mm \* 800 mm bipolar charging pad is made of AWG38 Litz wire with 800 strands. The TDK PC40 ferrite bars are used to support the charging pads. The system parameters are mentioned in Table 10.

The maximum power transfer capacity is [26]

$$P_{out} = |V_2 \times I_{sc}| = \frac{\omega I_1^2 M^2 Q^2}{L_2} \tag{33}$$

TABLE 10. Optimized parameters of 7.7 kW system [52].

Parameter	Variable	Value
Output Power	$P_{out}$	7.7 kW
Airgap Distance	Z	200 mm
Operating frequency	f	79 kHz
d.c. voltage limit	$V_{dc, max}$	$\leq 425$ V
Battery voltage limit	$V_b$	300 V – 450 V
Pad Dimension		600 mm * 800 mm
Litz wire		AWG 38 / 800 Strands
Efficiency (d.c. power to load)	$\eta_{max}$	95.66%
Efficiency (d.c. power to load)		95.39% (300 mm $\Delta x$ , $\Delta y$ )
Ferrite bars		TDK PC40
Dimension of the ferrite bar		60 mm * 16 mm * 8 mm
Power MOSFET (FCH041N60E)		N-Channel, 600 V, 77 A, 41 m $\Omega$

The output power can be controlled by varying transmitter current ( $I_1$ ), Mutual inductance (M), Quality factor (Q), system frequency (f), and inductance of the receiver coil. Hence, increasing the value of M is limited to charging pad dimensions, and receiver coil inductance and system resonant frequency is prefixed. Increasing the quality factor will lead to an increase in receiver-side reactive power. A wide range of power regulations is possible by controlling the primary current. But the efficiency will reduce and stress due to high current will increase. The current controller is preferred on the primary and secondary sides to regulate the system power [92]. The S-S compensation network is preferred for a full position-aligned system, and double-sided LCC compensation is preferred for a high position misaligned system. The circular and rectangular pads are favorable for transferring the maximum power with high efficiency. The circular pad is suitable for stationary charging, and the rectangular pad is preferable for dynamic charging. But the bipolar pads are preferable in a highly misalignment dynamic charging system.

The I-shaped ferrite core is favorable in several charging pads. The 600 V and 1200 V SiC MOSFET are preferable in power inverters due to their power-saving capability by decreasing switching losses and low on-state resistance. The power flow in grid-tied converter and voltage imbalance due to sudden rise in power demand are essential factors in a grid-integrated DWC system. An effective control technique is necessary to attain a smooth voltage profile and adequate power flow. Integration of renewable energy sources assists the grid-connected DWC system in achieving a smooth power demand curve. These renewable energy integrations can solve the peak power demand. Additionally, renewable energy sources are reducing grid utilization and its utilization cost.

TABLE 11. Comparison of S-S and D-LCC [98].

Diagram	S-S Compensation	D-LCC Compensation
	The resonant frequency is not depending on the coefficient of coupling and load conditions	The resonant frequency is not depending on the coefficient of coupling and load conditions
	Requires lesser components	Requires more components
	Output current is irrelevant to the various load changes. i.e., current source topology	Output current is irrelevant to the various load changes. i.e., current source topology
	Output current depends on input voltage, mutual inductance, and resonant frequency.	Output current depends on input voltage, mutual inductance, and resonant frequency.
	The power transfer capability of the compensation system increases with a decrease in the mutual inductance value. So, it requires vehicle coil detection or a power protection circuit.	The power transfer capability of the compensation system decreases with a decrease in the mutual inductance value. The $P_{max}$ is achieved in a completely aligned condition.
	The transferred power will be determined by resonant frequency, dimensions of the pad, and misalignment tolerance	The transferred power will be determined by resonant frequency, pad dimensions, misalignment tolerance, and additional inductances.
	The transmitter coil current can be determined directly.	The input voltage can determine the transmitter coil's constant current.
	Suitable for perfectly aligned position conditions	Favorable to maximum misalignment position conditions
	Maximum power will be transferred at maximum mutual inductance	Maximum power will be transferred at minimum mutual inductance
	Higher efficiency at maximum mutual inductance	Higher efficiency at minimum mutual inductance
	Higher voltage and current stress during x kW transfer	Low voltage and current stress during x Kw transfer

E. BIRDS VIEW

The parameters of the charging system, such as charging couplers, compensation networks, power converters, and detection systems are developed vastly by researchers.



- i. Regardless of the orientation, the charging couplers must transmit the optimum power. The vehicle pad's weight should be decreased without compromising the power transfer ratio. Utilizing the Litz coil will decrease the voltage drop of the pads. The charging pad's magnetic field emissions must be within allowed limits regardless of power rating.
  - ii. During power transmission, the compensation network must aid the charging couplers. It must also provide filtering and smooth switching assistance to the power converters. Additional harmonics or circulating currents should not be introduced via the network. For significant load variations, the network must be constructed with fewer passive components to transmit maximum power.
  - iii. The development of high-power, wide-bandgap semiconductors, such as SiC and GaN, inspires researchers to create a high-power WPT system. The power converter should perform under specific parameters such as soft switching, constant current, and voltage. The power converter's switching sequence must be synced with the vehicle's speed.
- The effect of wireless charging on the power grid was elaborated by many studies [67], [68], [69], [99].
- vi. The wireless charging station's demand may drastically affect the load profile of the existing electric grid distribution network. In addition, these modifications will affect the maximum permissible deployment level. It will cause the distribution network to break technical norms in terms of thermal limitations (line loads and transformers on the distribution side) and voltage restrictions ( $V_{\max}$  and  $V_{\min}$  at nodes).
  - v. Wireless charging influences the distribution network's functioning in terms of voltage and current profile (harmonics) and total network losses. The factors needed to estimate the influence of demand include the number of EV trips made on a given day, emergency charging by an EV user, EV traffic on highways, and vehicle speed.
  - vi. The significant changes in network voltage are compensated by an appropriate controller, such as a dual-active bridge converter.
  - vii. The energy storage devices may reduce demand fluctuation to an unlimited degree. However, to fully address this problem, demand-side management approaches are also necessary.
  - viii. Solar energy is a good way to reduce the overall impact of wireless charging on the grid. This is relevant in the morning when solar energy and traffic are naturally synchronized.
  - ix. Secure EV charging on the wireless charging lane is mandatory to avoid security threats [103], [104], [105] in an intelligent grid system. There should be proper communication between the user and the charging lane control center to predict the power demand to the grid.

The high-power wireless charging systems were elaborated by different researchers [17], [18], [100], [101], [102].

- i. The KRRI developed a 1-MW, 128-m long IPT charging system for electric trains with an efficiency of 82.7% for a 5-cm air gap. The induced a.c. the voltage on the rail was 31 V which is less than the permissible value. The developed system was tested at the electric train's 10 km/hr speed. And it is proven that the IPT charging systems can apply to railroads.
- ii. SAE has studied the 450 kW super DWC system and the system's d.c. parameters are 700 V, 300 A, and 180 kW. The power transmission distance is 1.3 m, and the vehicle speed is 5-155 km/hr. The d.c. power demand is satisfied by the high-volume storage devices. The parameters such as voltage, current, and power have maintained constant throughout the charging process. When driving at roughly 200 km/hr, the average utilized power is 95.6 kW, and the energy usage is 27 kWh. Under these circumstances, the vehicle could continue to operate if it could charge 29.3 kWh over a 12.7 km portion. The dynamic charging time is 3.81 minutes.
- iii. ORNL develops the 800 V, 200 kW system with an efficiency of 92%. The minimum ground clearance considered is 15 cm.

The high-power fast charging techniques eliminate the following obstacles to the development of wireless charging

- i. Restrictions on the cruising range of EVs
- ii. Decrease the waiting time of charging to zero
- iii. Decrease the weight of the vehicle by reducing the battery volume
- iv. Enhance driving enjoyment by eliminating EV power restrictions.

## F. FUTURE CONCERNS

Despite the immaturity of the wireless charging technology for an EV, several firms are developing charging solutions. Future concentration is necessary for the development of these wireless charging technologies. The following aspects might be considered in the wireless charging area from a future perspective.

### 1) CYBER SECURITY AND MACHINE LEARNING

- i. The risks to wireless charging systems from cyberspace should be prioritized. It will lessen the risks that were highlighted during the energy consumption billing procedure and communication from the vehicle to the charging lane.
- ii. The cloud server must be updated with the location and status of the WPT charging stations. The EV's onboard communication system must communicate with the roadside charging stations to convey the charging demand. In addition, the charging stations' energy demand must be reported to the grid system. The vehicle's position must be notified to roadside

DWC stations. In order to prevent the energy demand of the charging system from affecting the grid's stability communication is needed. This vehicle-to-station and station-to-grid communication protocol have a lot of security threats. Future research may be conducted using this protected communication infrastructure inside the wireless charging system.

- iii. Machine learning techniques will make the optimization process easier. The charging pad's optimization comprises dimensions of coil and ferrite. FEA datasets may be used to optimize the spacing between turns, the number of turns, and the inner/outer dimensions of a coil. In addition, the location of the ferrite, the number of ferrite strips, and the size of the ferrite were adjusted to decrease the charging pad's weight.

## 2) RES INTEGRATION

- i. By incorporating RES, the effect of wireless charging systems on the grid may be reduced. The charging profile will be improved, and the load demand curve may be smoothed by this integration.
- ii. In several countries, solar roads are developing technology. The DWC system may use the solar road's production. Additionally, the WPT system may be designed with different non-conventional energy sources based on geographical locations.
- iii. The standalone RES system will mitigate the effects of DWC on a grid system.
  - 1) When RES is connected with the grid system, load scheduling that incorporates wireless charging stations' consideration is essential.
  - iv. Therefore, load scheduling, demand side management, and route optimization are potential components of the on-road WPT charging system.

## 3) SUSTAINABLE ENERGY STORAGE

- i. The development of sustainable batteries will enhance the environmental friendliness of EVs.
- ii. Green transportation systems promote the advantages of fuel cells and ultracapacitors.
- iii. Currently, researchers are working to improve a battery management system for EVs that will significantly lessen the risks posed by energy storage devices.

## 4) THERMAL MANAGEMENT

- i. The thermal management system will work better if phase-change materials are introduced to the construction of the charging pad.
- ii. Many researchers are interested in developing an appropriate cooling system for power converters and charging pads as part of the thermal management for the high-power charging system.

## 5) HIGH-POWER CHARGING SYSTEM

- i. The high-power fast charging system must be developed without affecting the vehicle speed, and the

charging time must be reduced. The wireless charging system's efficiency might meet the level of plug-in charging.

- ii. The criteria might be considered by the researcher that multiple vehicles with different power ratings traveling on the charging lane at a time.
- iii. The high-power charging system's EMI/EMC concerns will encourage researchers to develop superior shielding solutions.
- iv. The compact high power high-frequency system is necessary to mitigate the EMI issues in the output response.

## 6) ECONOMICAL ASPECTS

- i. The installation cost of the DWC system may be minimized by optimizing the economic factors.
- ii. The optimization of material used to develop the WPT system will help the cost reduction
- iii. The cost saving is achievable by installing the WPT charging in high-traffic regions.

## VII. CONCLUSION

The main focus of this paper is to expose the parameters involved in grid-tied and PV-integrated DWC systems. The charging couplers involved in a dynamic charging system were tabulated and described. Those are used in the developed system. The different compensation networks, with their merits and demerits, are also discussed in this paper. The different power converters and their coil-energizing capability is discussed clearly. The driving pulses to the power converters are based on the vehicle's position. There may be sensors, or there may not be sensors. The detection circuit detects the presence of a foreign object, and the detection of the vehicle's position is also associated with it. The novel parameters of this article are this paper addresses the common challenges involved in the design of dynamic charging systems and challenges involved in grid-tied and PV-integrated dynamic charging systems. The step-by-step design process of the dynamic charging system is explained using a brief flow chart. The parameters involved in the existing developed system are addressed under case studies. This article helps to understand the factors involved in grid-tied and PV-integrated dynamic charging systems and how the dynamic charging system is designed.

## REFERENCES

- [1] *The Global Electric Vehicle Market in 2022—Virta*. Accessed: May 2, 2022. [Online]. Available: [https://www.virta.global/global-electric-vehiclemarket?\\_\\_hstc=51530422.a4119e1ebb088c79a85539e9c7f610ae.1651463928498.1651463928498.1&\\_\\_hssc=51530422.1.1651463928499&\\_\\_hsfp=3432168314&hsutk=a4119e1ebb088c79a85539e9c7f610ae&contentType=standard-page#six](https://www.virta.global/global-electric-vehiclemarket?__hstc=51530422.a4119e1ebb088c79a85539e9c7f610ae.1651463928498.1651463928498.1&__hssc=51530422.1.1651463928499&__hsfp=3432168314&hsutk=a4119e1ebb088c79a85539e9c7f610ae&contentType=standard-page#six)
- [2] *Introduction to Electric Vehicle Charging Method*. Accessed: May 2, 2022. [Online]. Available: <https://www.linkedin.com/pulse/introduction-electric-vehicle-charging-method-saket-dongre>
- [3] F. Ahmad, M. Saad Alam, I. Saad Alsaidan, and S. M. Shariff, "Battery swapping station for electric vehicles: Opportunities and challenges," *IET Smart Grid*, vol. 3, no. 3, pp. 280–286, Jun. 2020, doi: [10.1049/iet-stg.2019.0059](https://doi.org/10.1049/iet-stg.2019.0059).

- [4] F. Ahmad, M. S. Alam, and S. M. Shariff, "A cost-efficient energy management system for battery swapping station," *IEEE Syst. J.*, vol. 13, no. 4, pp. 4355–4364, Dec. 2019, doi: [10.1109/JSYST.2018.2890569](https://doi.org/10.1109/JSYST.2018.2890569).
- [5] M. Khalid, F. Ahmad, B. K. Panigrahi, and L. Al-Fagih, "A comprehensive review on advanced charging topologies and methodologies for electric vehicle battery," *J. Energy Storage*, vol. 53, Sep. 2022, Art. no. 105084, doi: [10.1016/j.est.2022.105084](https://doi.org/10.1016/j.est.2022.105084).
- [6] M. Khalid, F. Ahmad, and B. K. Panigrahi, "Design, simulation and analysis of a fast charging station for electric vehicles," *Energy Storage*, vol. 3, no. 6, Dec. 2021, doi: [10.1002/est.2.263](https://doi.org/10.1002/est.2.263).
- [7] W. Khan, A. Ahmad, F. Ahmad, and M. S. Alam, "A comprehensive review of fast charging infrastructure for electric vehicles," *Smart Sci.*, vol. 6, pp. 256–270, Jul. 2018, doi: [10.1080/23080477.2018.1437323](https://doi.org/10.1080/23080477.2018.1437323).
- [8] F. Ahmad, M. Khalid, and B. K. Panigrahi, "Development in energy storage system for electric transportation: A comprehensive review," *J. Energy Storage*, vol. 43, Nov. 2021, Art. no. 103153, doi: [10.1016/j.est.2021.103153](https://doi.org/10.1016/j.est.2021.103153).
- [9] S. M. Shariff, M. S. Alam, F. Ahmad, Y. Rafat, M. S. J. Asghar, and S. Khan, "System design and realization of a solar-powered electric vehicle charging station," *IEEE Syst. J.*, vol. 14, no. 2, pp. 2748–2758, Jun. 2020, doi: [10.1109/JSYST.2019.2931880](https://doi.org/10.1109/JSYST.2019.2931880).
- [10] S. Jeong, Y. J. Jang, and D. Kum, "Economic analysis of the dynamic charging electric vehicle," *IEEE Trans. Power Electron.*, vol. 30, no. 11, pp. 6368–6377, Nov. 2015, doi: [10.1109/TPEL.2015.2424712](https://doi.org/10.1109/TPEL.2015.2424712).
- [11] *Version-1 Prepa, Electric Vehicle Charging Infrastructure Implementation*, NITI Aayog, Ministry Power, Government India, India.
- [12] F. Faradjizadeh, M. Vilathgamuwa, D. Jovanovic, P. Jayathurathnage, G. Ledwich, and U. Madawala, "Expandable N-legged converter to drive closely spaced multitransmitter wireless power transfer systems for dynamic charging," *IEEE Trans. Power Electron.*, vol. 35, no. 4, pp. 3794–3806, Apr. 2020, doi: [10.1109/TPEL.2019.2939848](https://doi.org/10.1109/TPEL.2019.2939848).
- [13] S. Yuvaraja and R. Narayanamoorthi, "A five leg converter with multi-transmitter for an in-motion charging system," *J. Phys., Conf.*, vol. 2335, no. 1, Sep. 2022, Art. no. 012054, doi: [10.1088/1742-6596/2335/1/012054](https://doi.org/10.1088/1742-6596/2335/1/012054).
- [14] S. E. Shladover, "Highway electrification and automation," Inst. Transp. Stud., Univ. California, Berkeley, CA, USA, Tech. Rep. UCB-ITS-PRR-92-17, Dec. 1992.
- [15] K. Chen, K. W. E. Cheng, Y. Yang, and J. Pan, "A fast self-positioning-based optimal frequency control for inductive wireless power transfer systems without communication," *IEEE Trans. Ind. Electron.*, vol. 70, no. 1, pp. 334–343, Jan. 2023, doi: [10.1109/TIE.2022.3148758](https://doi.org/10.1109/TIE.2022.3148758).
- [16] BombardierRail. (Mar. 27, 2014). *World's First Electric Bus With Bombardier's PRIMOVE System Begins Revenue Service*. [Online]. Available: <https://bombardier.com/en/media/news/worlds-first-electric-bus-bombardiers-primove-system-begins-revenue-service>
- [17] J. H. Kim, B.-S. Lee, J.-H. Lee, S.-H. Lee, C.-B. Park, and S.-M. Jung, "Development of 1-MW inductive power transfer system for a high-speed train," *IEEE Trans. Ind. Electron.*, vol. 62, no. 10, pp. 6242–6250, Oct. 2015, doi: [10.1109/TIE.2015.2417122](https://doi.org/10.1109/TIE.2015.2417122).
- [18] Department of Energy's Oak Ridge National Laboratory. (Oct. 19, 2018). *ORNL Demonstrates 120-Kilowatt Wireless Charging for Vehicles*. [Online]. Available: <https://www.ornl.gov/news/ornl-demonstrates-120-kilowatt-wireless-charging-vehicles#:~:text=19%2C%202018%2E2%80%94Researchers%20at%20the,a%20gas%20station%20fill%2D>
- [19] *Application of Shaped Magnetic Field in Resonance (SMFIR) Technology to Future Urban Transportation*, Garduation School Green Transp., KAIST, Daejeon, South Korea.
- [20] A. A. S. Mohamed, A. A. Shaier, H. Metwally, and S. I. Selem, "A comprehensive overview of inductive pad in electric vehicles stationary charging," *Appl. Energy*, vol. 262, Mar. 2020, Art. no. 114584, doi: [10.1016/j.apenergy.2020.114584](https://doi.org/10.1016/j.apenergy.2020.114584).
- [21] D. De Marco, A. Dolar, M. Longo, and W. Yaici, "Design and performance analysis of pads for dynamic wireless charging of EVs using the finite element method," *Energies*, vol. 12, no. 21, p. 4139, Oct. 2019, doi: [10.3390/en12214139](https://doi.org/10.3390/en12214139).
- [22] D. Patil, M. K. McDonough, J. M. Miller, B. Fahimi, and P. T. Balsara, "Wireless power transfer for vehicular applications: Overview and challenges," *IEEE Trans. Transport. Electric.*, vol. 4, no. 1, pp. 3–37, Mar. 2018, doi: [10.1109/TTE.2017.2780627](https://doi.org/10.1109/TTE.2017.2780627).
- [23] G. Yang, K. Song, Y. Sun, X. Huang, J. Li, Y. Guo, H. Zhang, Q. Zhang, R. Lu, and C. Zhu, "Interoperability improvement for rectangular pad and DD pad of wireless electric vehicle charging system based on adaptive position adjustment," *IEEE Trans. Ind. Appl.*, vol. 57, no. 3, pp. 2613–2624, May 2021, doi: [10.1109/TIA.2021.3056639](https://doi.org/10.1109/TIA.2021.3056639).
- [24] M. Budhia, J. T. Boys, G. A. Covic, and C.-Y. Huang, "Development of a single-sided flux magnetic coupler for electric vehicle IPT charging systems," *IEEE Trans. Ind. Electron.*, vol. 60, no. 1, pp. 318–328, Jan. 2013, doi: [10.1109/TIE.2011.2179274](https://doi.org/10.1109/TIE.2011.2179274).
- [25] T.-D. Nguyen, S. Li, W. Li, and C. C. Mi, "Feasibility study on bipolar pads for efficient wireless power chargers," in *Proc. IEEE Appl. Power Electron. Conf. Exposit. (APEC)*, Mar. 2014, pp. 1676–1682, doi: [10.1109/APEC.2014.6803531](https://doi.org/10.1109/APEC.2014.6803531).
- [26] J. T. Boys, G. A. Covic, and A. W. Green, "Stability and control of inductively coupled power transfer systems," *IEE Proc. Electr. Power Appl.*, vol. 147, no. 1, pp. 37–43, 2000, doi: [10.1049/ip-epa:20000017](https://doi.org/10.1049/ip-epa:20000017).
- [27] H. Jafari, T. O. Olowu, M. Mahmoudi, and A. Sarwat, "Optimal design of IPT bipolar power pad for roadway-powered EV charging systems," *IEEE Can. J. Electr. Comput. Eng.*, vol. 44, no. 3, pp. 350–355, Jul. 2021, doi: [10.1109/ICJECE.2021.3075639](https://doi.org/10.1109/ICJECE.2021.3075639).
- [28] *Wireless Power Transfer for Light-Duty Plug-in/Electric Vehicles and Alignment Methodology J2954\_202010*, SAE International, Warrendale, PA, USA, Oct. 2020.
- [29] *Steinmetz's Equation—Wikipedia*. Accessed: May 5, 2022. [Online]. Available: [https://en.wikipedia.org/wiki/Steinmetz%27s\\_equation](https://en.wikipedia.org/wiki/Steinmetz%27s_equation)
- [30] G. Ziegelberger, "Guidelines for limiting exposure to electromagnetic fields (100 kHz to 300 GHz)," *Health Phys.*, vol. 118, no. 5, pp. 483–524, May 2020, doi: [10.1097/HP.0000000000001210](https://doi.org/10.1097/HP.0000000000001210).
- [31] V. Shevchenko, S. Member, O. Husev, and S. Member, "Compensation topologies in IPT systems: Standards, requirements, classification, analysis, comparison and application," *IEEE Access*, vol. 7, pp. 120559–120580, 2019, doi: [10.1109/ACCESS.2019.2937891](https://doi.org/10.1109/ACCESS.2019.2937891).
- [32] A. Mahesh, B. Chokkalingam, and L. Mihet-Popa, "Inductive wireless power transfer charging for electric vehicles—A review," *IEEE Access*, vol. 9, pp. 137667–137713, 2021, doi: [10.1109/ACCESS.2021.3116678](https://doi.org/10.1109/ACCESS.2021.3116678).
- [33] W. Zhang and C. C. Mi, "Compensation topologies of high-power wireless power transfer systems," *IEEE Trans. Veh. Technol.*, vol. 65, no. 6, pp. 4768–4778, Jun. 2016, doi: [10.1109/TVT.2015.2454292](https://doi.org/10.1109/TVT.2015.2454292).
- [34] R. Mai, Y. Chen, Y. Li, Y. Zhang, G. Cao, and Z. He, "Inductive power transfer for massive electric bicycles charging based on hybrid topology switching with a single inverter," *IEEE Trans. Power Electron.*, vol. 32, no. 8, pp. 5897–5906, Aug. 2017, doi: [10.1109/TPEL.2017.2654360](https://doi.org/10.1109/TPEL.2017.2654360).
- [35] T. Fujita, T. Yasuda, and H. Akagi, "A dynamic wireless power transfer system applicable to a stationary system," *IEEE Trans. Ind. Appl.*, vol. 53, no. 4, pp. 3748–3757, Jul. 2017, doi: [10.1109/TIA.2017.2680400](https://doi.org/10.1109/TIA.2017.2680400).
- [36] B.-V. Vu, V.-T. Phan, M. Dahidah, and V. Pickert, "Multiple output inductive charger for electric vehicles," *IEEE Trans. Power Electron.*, vol. 34, no. 8, pp. 7350–7368, Aug. 2019, doi: [10.1109/TPEL.2018.2882945](https://doi.org/10.1109/TPEL.2018.2882945).
- [37] Y. Guo, L. Wang, Q. Zhu, C. Liao, and F. Li, "Switch-on modeling and analysis of dynamic wireless charging system used for electric vehicles," *IEEE Trans. Ind. Electron.*, vol. 63, no. 10, pp. 6568–6579, Oct. 2016, doi: [10.1109/TIE.2016.2557302](https://doi.org/10.1109/TIE.2016.2557302).
- [38] H. Zhou, J. Chen, Q. Deng, F. Chen, A. Zhu, W. Hu, and X. Gao, "Input-series output-equivalent-parallel multi-inverter system for high-voltage and high-power wireless power transfer," *IEEE Trans. Power Electron.*, vol. 36, no. 1, pp. 228–238, Jan. 2021, doi: [10.1109/TPEL.2020.3000244](https://doi.org/10.1109/TPEL.2020.3000244).
- [39] E. S. Lee, M. Y. Kim, S. M. Kang, and S. H. Han, "Segmented IPT coil design for continuous multiple charging of an electrified monorail system," *IEEE Trans. Power Electron.*, vol. 37, no. 3, pp. 3636–3649, Mar. 2022, doi: [10.1109/TPEL.2021.3115511](https://doi.org/10.1109/TPEL.2021.3115511).
- [40] M. H. Rashid, *Power Electronics: Devices, Circuits, and Applications*. London, U.K.: Pearson.
- [41] S. Yuvaraja, J. S. Mohamed Ali, and D. Almakhlis, "A comprehensive review of the on-road wireless charging system for E-mobility applications," *Frontiers Energy Res.*, vol. 10, Jul. 2022, doi: [10.3389/fenrg.2022.926270](https://doi.org/10.3389/fenrg.2022.926270).
- [42] Y. Zhang, Z. Yan, J. Zhu, S. Li, and C. Mi, "A review of foreign object detection (FOD) for inductive power transfer systems," *eTransportation*, vol. 1, Aug. 2019, Art. no. 100002, doi: [10.1016/j.etrans.2019.04.002](https://doi.org/10.1016/j.etrans.2019.04.002).
- [43] M. Budhia, G. A. Covic, and J. T. Boys, "Design and optimization of circular magnetic structures for lumped inductive power transfer systems," *IEEE Trans. Power Electron.*, vol. 26, no. 11, pp. 3096–3108, Nov. 2011, doi: [10.1109/TPEL.2011.2143730](https://doi.org/10.1109/TPEL.2011.2143730).
- [44] C. Panchal, S. Stegen, and J. Lu, "Review of static and dynamic wireless electric vehicle charging system," *Eng. Sci. Technol. Int. J.*, vol. 21, no. 5, pp. 922–937, 2018, doi: [10.1016/j.jestech.2018.06.015](https://doi.org/10.1016/j.jestech.2018.06.015).
- [45] I. U. Castillo-Zamora, P. S. Huynh, D. Vincent, F. J. Perez-Pinal, M. A. Rodriguez-Licea, and S. S. Williamson, "Hexagonal geometry coil for a WPT high-power fast charging application," *IEEE Trans. Transport. Electric.*, vol. 5, no. 4, pp. 946–956, Dec. 2019, doi: [10.1109/TTE.2019.2941636](https://doi.org/10.1109/TTE.2019.2941636).



- [46] R. Narayanamoorthi, V. Juliet, S. Padmanaban, L. Mihet-Popa, and C. Bharatiraja, "Frequency splitting elimination and cross-coupling rejection of wireless power transfer to multiple dynamic receivers," *Appl. Sci.*, vol. 8, no. 2, p. 179, Jan. 2018, doi: [10.3390/app8020179](https://doi.org/10.3390/app8020179).
- [47] R. Narayanamoorthi and A. V. Juliet, "Capacitor-less high-strength resonant wireless power transfer using open bifilar spiral coil," *IEEE Trans. Appl. Supercond.*, vol. 29, no. 1, pp. 1–8, Jan. 2019, doi: [10.1109/TASC.2018.2848268](https://doi.org/10.1109/TASC.2018.2848268).
- [48] A. Ahmad, M. S. Alam, and A. A. S. Mohamed, "Design and interoperability analysis of quadruple pad structure for electric vehicle wireless charging application," *IEEE Trans. Transport. Electrific.*, vol. 5, no. 4, pp. 934–945, Dec. 2019, doi: [10.1109/TTE.2019.2929443](https://doi.org/10.1109/TTE.2019.2929443).
- [49] S. Kim, G. A. Covic, and J. T. Boys, "Tripolar pad for inductive power transfer systems for EV charging," *IEEE Trans. Power Electron.*, vol. 32, no. 7, pp. 5045–5057, Jul. 2017, doi: [10.1109/TPEL.2016.2606893](https://doi.org/10.1109/TPEL.2016.2606893).
- [50] S. Wang, J. Chen, Z. Hu, C. Rong, and M. Liu, "Optimisation design for series-series dynamic WPT system maintaining stable transfer power," *IET Power Electron.*, vol. 10, no. 9, pp. 987–995, Jul. 2017, doi: [10.1049/iet-pel.2016.0839](https://doi.org/10.1049/iet-pel.2016.0839).
- [51] Y. Wang, S. Zhao, H. Zhang, and F. Lu, "High-efficiency bilateral S-SP compensated multiloop IPT system with constant-voltage outputs," *IEEE Trans. Ind. Informat.*, vol. 18, no. 2, pp. 901–910, Feb. 2022, doi: [10.1109/TII.2021.3072394](https://doi.org/10.1109/TII.2021.3072394).
- [52] S. Li, W. Li, J. Deng, T. D. Nguyen, and C. C. Mi, "A double-sided LCC compensation network and its tuning method for wireless power transfer," *IEEE Trans. Veh. Technol.*, vol. 64, no. 6, pp. 2261–2273, Jun. 2015, doi: [10.1109/TVT.2014.2347006](https://doi.org/10.1109/TVT.2014.2347006).
- [53] Y. Yao, Y. Wang, X. Liu, F. Lin, and D. Xu, "A novel parameter tuning method for a double-sided LCL Compensated WPT system with better comprehensive performance," *IEEE Trans. Power Electron.*, vol. 33, no. 10, pp. 8525–8536, Oct. 2018, doi: [10.1109/TPEL.2017.2778255](https://doi.org/10.1109/TPEL.2017.2778255).
- [54] Z. Yan, Y. Zhang, B. Song, K. Zhang, T. Kan, and C. Mi, "An LCC-P compensated wireless power transfer system with a constant current output and reduced receiver size," *Energies*, vol. 12, no. 1, p. 172, Jan. 2019, doi: [10.3390/en12010172](https://doi.org/10.3390/en12010172).
- [55] J. Yang, X. Zhang, K. Zhang, X. Cui, C. Jiao, and X. Yang, "Design of LCC-S compensation topology and optimization of misalignment tolerance for inductive power transfer," *IEEE Access*, vol. 8, pp. 191309–191318, 2020, doi: [10.1109/ACCESS.2020.3032563](https://doi.org/10.1109/ACCESS.2020.3032563).
- [56] J. Yang, X. Zhang, K. Zhang, X. Cui, C. Jiao, and X. Yang, "An LCC-SP compensated inductive power transfer system and design considerations for enhancing misalignment tolerance," *IEEE Access*, vol. 8, pp. 193285–193296, 2020, doi: [10.1109/ACCESS.2020.3032793](https://doi.org/10.1109/ACCESS.2020.3032793).
- [57] C. Xiao, B. Cao, and C. Liao, "A fast construction method of resonance compensation network for electric vehicle wireless charging system," *IEEE Trans. Instrum. Meas.*, vol. 70, pp. 1–9, 2021, doi: [10.1109/TIM.2021.3055783](https://doi.org/10.1109/TIM.2021.3055783).
- [58] L. Yang, X. Li, S. Liu, Z. Xu, and C. Cai, "Analysis and design of an LCCC/S-compensated WPT system with constant output characteristics for battery charging applications," *IEEE J. Emerg. Sel. Topics Power Electron.*, vol. 9, no. 1, pp. 1169–1180, Feb. 2021, doi: [10.1109/JESTPE.2020.2971583](https://doi.org/10.1109/JESTPE.2020.2971583).
- [59] N. S. González-Santini, H. Zeng, Y. Yu, and F. Z. Peng, "Z-source resonant converter with power factor correction for wireless power transfer applications," *IEEE Trans. Power Electron.*, vol. 31, no. 11, pp. 7691–7700, Nov. 2016, doi: [10.1109/TPEL.2016.2560174](https://doi.org/10.1109/TPEL.2016.2560174).
- [60] V. Z. Barsari, D. J. Thrimawithana, and G. A. Covic, "An inductive coupler array for in-motion wireless charging of electric vehicles," *IEEE Trans. Power Electron.*, vol. 36, no. 9, pp. 9854–9863, Sep. 2021, doi: [10.1109/TPEL.2021.3058666](https://doi.org/10.1109/TPEL.2021.3058666).
- [61] P. S. Huynh and S. S. Williamson, "Analysis and design of soft-switching active-clamping half-bridge boost inverter for inductive wireless charging applications," *IEEE Trans. Transport. Electrific.*, vol. 5, no. 4, pp. 1027–1039, Dec. 2019, doi: [10.1109/TTE.2019.2930199](https://doi.org/10.1109/TTE.2019.2930199).
- [62] J. Liu, Q. Deng, W. Wang, and Z. Li, "Modeling and control of inverter zero-voltage-switching for inductive power transfer system," *IEEE Access*, vol. 7, pp. 139885–139894, 2019, doi: [10.1109/ACCESS.2019.2943398](https://doi.org/10.1109/ACCESS.2019.2943398).
- [63] X.-J. Ge, Y. Sun, Z.-H. Wang, and C.-S. Tang, "Dual-independent-output inverter for dynamic wireless power transfer system," *IEEE Access*, vol. 7, pp. 107320–107333, 2019, doi: [10.1109/ACCESS.2019.2933017](https://doi.org/10.1109/ACCESS.2019.2933017).
- [64] W. V. Wang and D. J. Thrimawithana, "A novel converter topology for a primary-side controlled wireless EV charger with a wide operation range," *IEEE J. Emerg. Sel. Topics Ind. Electron.*, vol. 1, no. 1, pp. 36–45, Jul. 2020, doi: [10.1109/jestie.2020.3003357](https://doi.org/10.1109/jestie.2020.3003357).
- [65] R. Zeng, V. P. Galigekere, O. C. Onar, and B. Ozpineci, "Improved control strategy of grid interface for EV high-power dynamic wireless charging," in *Proc. IEEE Appl. Power Electron. Conf. Exposit. (APEC)*, Jun. 2021, pp. 2574–2579, doi: [10.1109/APEC42165.2021.9487243](https://doi.org/10.1109/APEC42165.2021.9487243).
- [66] L. Xu, D. Zhi, and L. Yao, "Direct power control of grid connected voltage source converters," in *Proc. IEEE Power Eng. Soc. General Meeting*, Jun. 2007, pp. 1–6.
- [67] R. Zeng, V. P. Galigekere, O. C. Onar, and B. Ozpineci, "Grid integration and impact analysis of high-power dynamic wireless charging system in distribution network," *IEEE Access*, vol. 9, pp. 6746–6755, 2021, doi: [10.1109/ACCESS.2021.3049186](https://doi.org/10.1109/ACCESS.2021.3049186).
- [68] S. Debnath, A. Foote, O. C. Onar, and M. Chinthavali, "Grid impact studies from dynamic wireless charging in smart automated highways," in *Proc. IEEE Transp. Electrific. Conf. Expo. (ITEC)*, Jun. 2018, pp. 650–655, doi: [10.1109/ITEC.2018.8450149](https://doi.org/10.1109/ITEC.2018.8450149).
- [69] T. Theodoropoulos, A. Amditis, J. Sallán, H. Bludszweit, and B. Berseneff, "Impact of dynamic EV wireless charging on the grid," in *Proc. IEEE Int. Electric Vehicle Conf. (IEVC)*, Dec. 2014, pp. 1–7, doi: [10.1109/IEVC.2014.7056234](https://doi.org/10.1109/IEVC.2014.7056234).
- [70] F. Birol. (2021). *Global Energy Review 2021*. IEA Executive Director. [Online]. Available: <https://www.iea.org/reports/global-energy-review-2021>
- [71] G. R. Chandra Mouli, P. Van Duijzen, F. Grazian, A. Jamodkar, P. Bauer, and O. Isabella, "Sustainable E-bike charging station that enables AC, DC and wireless charging from solar energy," *Energies*, vol. 13, no. 14, p. 3549, Jul. 2020, doi: [10.3390/en13143549](https://doi.org/10.3390/en13143549).
- [72] T. Celik and H. Kusetoğullari, "Solar-powered automated road surveillance system for speed violation detection," *IEEE Trans. Ind. Electron.*, vol. 57, no. 9, pp. 3216–3227, Sep. 2010, doi: [10.1109/TIE.2009.2038395](https://doi.org/10.1109/TIE.2009.2038395).
- [73] *Indian Highway to Host 250 MW Solar Plant—PV Magazine International*. Accessed: May 16, 2022. [Online]. Available: <https://www.pv-magazine.com/2021/06/08/indian-highway-to-host-250-mw-solar-plant/>
- [74] B. Zhou, J. Pei, J. K. Calautit, J. Zhang, and F. Guo, "Solar self-powered wireless charging pavement—A review on photovoltaic pavement and wireless charging for electric vehicles," *Sustain. Energy Fuels*, vol. 5, no. 20, pp. 5139–5159, Oct. 2021, doi: [10.1039/d1se00739d](https://doi.org/10.1039/d1se00739d).
- [75] H. Humfrey, H. Sun, and J. Jiang, "Dynamic charging of electric vehicles integrating renewable energy: A multi-objective optimisation problem," *IET Smart Grid*, vol. 2, no. 2, pp. 250–259, Jun. 2019, doi: [10.1049/iet-stg.2018.0066](https://doi.org/10.1049/iet-stg.2018.0066).
- [76] X. Mou, Y. Zhang, J. Jiang, and H. Sun, "Achieving low carbon emission for dynamically charging electric vehicles through renewable energy integration," *IEEE Access*, vol. 7, pp. 118876–118888, 2019, doi: [10.1109/ACCESS.2019.2936935](https://doi.org/10.1109/ACCESS.2019.2936935).
- [77] R. Zeng, V. Galigekere, O. Onar, and B. Ozpineci, "Optimized renewable energy integration for EV high-power dynamic wireless charging systems," in *Proc. IEEE Power Energy Soc. Innov. Smart Grid Technol. Conf. (ISGT)*, Feb. 2021, pp. 1–5, doi: [10.1109/ISGT49243.2021.9372265](https://doi.org/10.1109/ISGT49243.2021.9372265).
- [78] M. Shahidul Haque, M. Mohammad, J. L. Pries, and S. Choi, "Comparison of 22 kHz and 85 kHz 50 kW wireless charging system using Si and SiC switches for electric vehicle," in *Proc. IEEE 6th Workshop Wide Bandgap Power Devices Appl. (WiPDA)*, Oct. 2018, pp. 192–198. [Online]. Available: <http://energy.gov/downloads/doe-public>
- [79] R. Bosshard and J. W. Kolar, "Multi-objective optimization of 50 kW/85 kHz IPT system for public transport," *IEEE J. Emerg. Sel. Topics Power Electron.*, vol. 4, no. 4, pp. 1370–1382, Dec. 2016, doi: [10.1109/JESTPE.2016.2598755](https://doi.org/10.1109/JESTPE.2016.2598755).
- [80] R. Bosshard, U. Iruretagoyena, and J. W. Kolar, "Comprehensive evaluation of rectangular and double-D coil geometry for 50 kW/85 kHz IPT system," *IEEE J. Emerg. Sel. Topics Power Electron.*, vol. 4, no. 4, pp. 1406–1415, Dec. 2016, doi: [10.1109/JESTPE.2016.2600162](https://doi.org/10.1109/JESTPE.2016.2600162).
- [81] R. Bosshard and J. W. Kolar, "All-SiC 9.5 kW/dm<sup>3</sup> on-board power electronics for 50 kW/85 kHz automotive IPT system," *IEEE J. Emerg. Sel. Topics Power Electron.*, vol. 5, no. 1, pp. 419–431, Mar. 2017, doi: [10.1109/JESTPE.2016.2624285](https://doi.org/10.1109/JESTPE.2016.2624285).
- [82] B. J. Varghese, A. Kamineni, N. Roberts, M. Halling, D. J. Thrimawithana, and R. A. Zane, "Design considerations for 50 kW dynamic wireless charging with concrete-embedded coils," in *Proc. IEEE PELS Workshop Emerg. Technol., Wireless Power Transf. (WoW)*, Nov. 2020, pp. 40–44, doi: [10.1109/WoW47795.2020.9291275](https://doi.org/10.1109/WoW47795.2020.9291275).



- [83] J. Pries, V. P. N. Galigekere, O. C. Onar, and G.-J. Su, "A 50-kW three-phase wireless power transfer system using bipolar windings and series resonant networks for rotating magnetic fields," *IEEE Trans. Power Electron.*, vol. 35, no. 5, pp. 4500–4517, May 2020, doi: [10.1109/TPEL.2019.2942065](https://doi.org/10.1109/TPEL.2019.2942065).
- [84] M. Mohammad, J. L. Pries, O. C. Onar, V. P. Galigekere, G. J. Su, and J. Wilkins, "Three-phase LCC-LCC compensated 50-kW wireless charging system with non-zero interphase coupling," in *Proc. IEEE Appl. Power Electron. Conf. Expo. (APEC)*, Jun. 2021, pp. 456–462, doi: [10.1109/APEC42165.2021.9487224](https://doi.org/10.1109/APEC42165.2021.9487224).
- [85] M. Mohammad, J. L. Pries, O. C. Onar, V. P. Galigekere, and G. J. Su, "Shield design for 50 kW three-phase wireless charging system," in *Proc. IEEE Energy Convers. Congr. Expo. (ECCE)*, Oct. 2020, pp. 842–849, doi: [10.1109/ECCE44975.2020.9236371](https://doi.org/10.1109/ECCE44975.2020.9236371).
- [86] A. U. Ibrahim, W. Zhong, and M. D. Xu, "A 50-kW three-channel wireless power transfer system with low stray magnetic field," *IEEE Trans. Power Electron.*, vol. 36, no. 9, pp. 9941–9954, Sep. 2021, doi: [10.1109/TPEL.2021.3064373](https://doi.org/10.1109/TPEL.2021.3064373).
- [87] J. Schneider, R. Carlson, J. Sirota, and R. Sutton, "Validation of wireless power transfer up to 11 kW based on SAE J2954 with bench and vehicle testing," SAE, Warrendale, PA, USA, Tech. Papers 2019-01-0868, Apr. 2019, doi: [10.4271/2019-01-0868](https://doi.org/10.4271/2019-01-0868).
- [88] M. Xiong, H. Dai, Q. Li, Z. Jiang, Z. Luo, and X. Wei, "Design of the LCC-SP topology with a current doubler for 11-kW wireless charging system of electric vehicles," *IEEE Trans. Transport. Electrification*, vol. 7, no. 4, pp. 2128–2142, Dec. 2021, doi: [10.1109/TTE.2021.3074007](https://doi.org/10.1109/TTE.2021.3074007).
- [89] W. Shi, F. Grazian, S. Bandyopadhyay, J. Dong, T. B. Soeiro, and P. Bauer, "Analysis of dynamic charging performances of optimized inductive power transfer couplers," in *Proc. IEEE 19th Int. Power Electron. Motion Control Conf. (PEMC)*, Apr. 2021, pp. 751–756, doi: [10.1109/PEMC48073.2021.9432541](https://doi.org/10.1109/PEMC48073.2021.9432541).
- [90] W. V. Wang, D. J. Thirumawithana, B. Riar, and R. Zane, "A novel integrated boost modular multilevel converter for high power wireless EV charging," in *Proc. IEEE Energy Convers. Congr. Expo. (ECCE)*, 2018, pp. 81–88, doi: [10.1109/ECCE.2018.8557404](https://doi.org/10.1109/ECCE.2018.8557404).
- [91] Y. Wang, M. Xiong, X. Wang, Q. Li, Z. Jiang, X. Wei, and H. Dai, "Research on 11 kW wireless charging system for electric vehicle based on LCC-SP topology and current doubler," in *Proc. IEEE Energy Convers. Congr. Exposit. (ECCE)*, Oct. 2020, pp. 820–827, doi: [10.1109/ECCE44975.2020.9235377](https://doi.org/10.1109/ECCE44975.2020.9235377).
- [92] R. Tavakoli and Z. Pantic, "Analysis, design, and demonstration of a 25-kW dynamic wireless charging system for roadway electric vehicles," *IEEE J. Emerg. Sel. Topics Power Electron.*, vol. 6, no. 3, pp. 1379–1393, Sep. 2018, doi: [10.1109/JESTPE.2017.2761763](https://doi.org/10.1109/JESTPE.2017.2761763).
- [93] A. A. S. Mohamed, A. Meintz, P. Schrafel, and A. Calabro, "Testing and assessment of EMFs and touch currents from 25-kW IPT system for medium-duty EVs," *IEEE Trans. Veh. Technol.*, vol. 68, no. 8, pp. 7477–7487, Aug. 2019, doi: [10.1109/TVT.2019.2920827](https://doi.org/10.1109/TVT.2019.2920827).
- [94] *Methods of Measurement of Touch Current and Protective Conductor Current*, Bureau of Indian Standards, document IS/IEC 60990, 1999.
- [95] W. Shi, J. Dong, T. B. Soeiro, C. Riekerk, F. Grazian, G. Yu, and P. Bauer, "Design of a highly efficient 20-kW inductive power transfer system with improved misalignment performance," *IEEE Trans. Transport. Electrification*, vol. 8, no. 2, pp. 2384–2399, Jun. 2022, doi: [10.1109/TTE.2021.3133759](https://doi.org/10.1109/TTE.2021.3133759).
- [96] O. C. Onar, M. Chinthavali, S. L. Campbell, L. E. Seiber, C. P. White, and V. P. Galigekere, "Modeling, simulation, and experimental verification of a 20-kW series-series wireless power transfer system for a toyota RAV4 electric vehicle," in *Proc. IEEE Transp. Electrification Conf. Expo. (ITEC)*, Jun. 2018, pp. 436–441, doi: [10.1109/ITEC.2018.8450085](https://doi.org/10.1109/ITEC.2018.8450085).
- [97] F. Grazian, W. Shi, T. B. Soeiro, J. Dong, P. van Duijsen, and P. Bauer, "Compensation network for a 7.7 kW wireless charging system that uses standardized coils," in *Proc. IEEE Int. Symp. Circuits Syst. (ISCAS)*, 2020, pp. 1–5, doi: [10.1109/ISCAS45731.2020.9181016](https://doi.org/10.1109/ISCAS45731.2020.9181016).
- [98] W. Li, H. Zhao, J. Deng, S. Li, and C. C. Mi, "Comparison study on SS and double-sided LCC compensation topologies for EV/PHEV wireless chargers," *IEEE Trans. Veh. Technol.*, vol. 65, no. 6, pp. 4429–4439, Jun. 2016, doi: [10.1109/TVT.2015.2479938](https://doi.org/10.1109/TVT.2015.2479938).
- [99] I. Karakitsios, E. Karfopoulos, and N. Hatziargyriou, "Impact of dynamic and static fast inductive charging of electric vehicles on the distribution network," *Electr. Power Syst. Res.*, vol. 140, pp. 107–115, Nov. 2016, doi: [10.1016/j.epsr.2016.06.034](https://doi.org/10.1016/j.epsr.2016.06.034).
- [100] T. Tajima, H. Tanaka, T. Fukuda, and Y. Nakasato, "Study of high power dynamic charging system," SAE, Warrendale, PA, USA, Tech. Papers 2017-01-1245, Mar. 2017, doi: [10.4271/2017-01-1245](https://doi.org/10.4271/2017-01-1245).
- [101] T. Tajima and H. Tanaka, "Study of 450-kW ultra power dynamic charging system," SAE, Warrendale, PA, USA, Tech. Papers 2018-01-1343, Apr. 2018, doi: [10.4271/2018-01-1343](https://doi.org/10.4271/2018-01-1343).
- [102] L. Xue, V. Galigekere, G.-J. Su, R. Zeng, M. Mohammad, and E. Gurpinar, "Design and analysis of a 200 kW dynamic wireless charging system for electric vehicles," in *Proc. IEEE Applied Power Electron. Conf. Expo. (APEC)*, Mar. 2022, pp. 1096–1103, doi: [10.1109/APEC43599.2022.9773670](https://doi.org/10.1109/APEC43599.2022.9773670).
- [103] Y. Wang, H. T. Luan, Z. Su, N. Zhang, and A. Benslimane, "A secure and efficient wireless charging scheme for electric vehicles in vehicular energy networks," *IEEE Trans. Veh. Technol.*, vol. 71, no. 2, pp. 1491–1508, Feb. 2022, doi: [10.1109/TVT.2021.3131776](https://doi.org/10.1109/TVT.2021.3131776).
- [104] Y. Wang, Z. Su, J. Li, N. Zhang, K. Zhang, K.-K.-R. Choo, and Y. Liu, "Blockchain-based secure and cooperative private charging pile sharing services for vehicular networks," *IEEE Trans. Veh. Technol.*, vol. 71, no. 2, pp. 1857–1874, Feb. 2022, doi: [10.1109/TVT.2021.3131744](https://doi.org/10.1109/TVT.2021.3131744).
- [105] Y. Wang, Z. Su, N. Zhang, and R. Li, "Mobile wireless rechargeable UAV networks: Challenges and solutions," *IEEE Commun. Mag.*, vol. 60, no. 3, pp. 33–39, Mar. 2022, doi: [10.1109/MCOM.001.2100731](https://doi.org/10.1109/MCOM.001.2100731).



**YUVARAJA SHANMUGAM** received the B.E. degree in electrical and electronics engineering from the Dhanalakshmi College of Engineering, Chennai, and the M.Tech. degree in power electronics and drives from SRM University, Kattankulathur, Chennai. He is a Research Scholar with the Department of EEE, SRM University. His research interests include wireless power transfer, resonant inductive power charging, and green transportation. He is a Lifetime Member of IETE and IAENG.



**NARAYANAMOORTHI R** received the bachelor's degree in electrical engineering and the master's degree in control and instrumentation from Anna University, India, in 2009 and 2011, respectively, and the doctoral degree from the SRM Institute of Science and Technology, India, in 2019. He is an Associate Professor with the Department of Electrical and Electronics Engineering, SRM Institute of Science and Technology. His research interests include wireless power transfer, electric vehicles, power electronics, artificial intelligence and machine learning in renewable energy systems, and embedded system for smart sensors.



**PRADEEP VISHNURAM** received the B.E. degree from the J. J. College of Engineering and Technology, Trichy, in 2012, the M.E. degree in power electronics and drives from the Jerusalem College of Engineering, Chennai, in 2014, and the Ph.D. degree from VIT, Chennai, India, in 2022. He is an Assistant Professor with the Department of Electrical and Electronics Engineering, SRM Institute of Science and Technology, Chennai. He has published more than 45 research articles in various renowned international journals. His research interests include resonant converters for induction heating, wireless power transfer, solar MPPT, intelligent controllers, and high power factor rectifiers. He is a reviewer of various reputed journals.



**MOHIT BAJAJ** received the B.Tech. degree in core electrical engineering from the Gurukula Kangri Vishwavidyalaya (one of the oldest and premier universities), Haridwar, India, the master's degree in electrical engineering from the Motilal Nehru National Institute of Technology (one of the premier engineering institutes), Allahabad, India, in the disciplines of power electronics and ASIC design, and the Ph.D. degree in electrical engineering from the National Institute of Technology,

Delhi, India, in 2022. He has published extensively in his research areas. He has authored more than 100 research publications in reputed journals, international conferences, and book chapters. He has published more than 80 research articles in SCI/SCIE indexed journals of reputed publishers, such as IEEE, Elsevier, Wiley, Taylor and Francis, Springer, etc. Much work is in the process of publication. His primary research interests include electric vehicles, renewable energy sources, distributed generation, power quality, and smart grids. He also serves as a Reviewer for many international journals of repute, such as IEEE TRANSACTIONS/Journals. He is ranked among the World's Top 2% Scientists as per the recent study conducted by researchers of ICSR Laboratory, Elsevier B.V., and Stanford University, USA.



**KAREEM M. ABORAS** received the B.Sc., M.Sc., and Ph.D. degrees in electrical engineering from the Faculty of Engineering, Alexandria University, Alexandria, Egypt, in 2010, 2015, and 2020, respectively. His Ph.D. research work was focused on the performance enhancement of renewable energy conversion systems. Currently, he is an Assistant Professor with the Electrical Power and Machines Department, Faculty of Engineering, Alexandria University. His research interests include power electronics, control, drives, power systems, and renewable energy systems. He is a reviewer of the IET journal.



**PADMANABH THAKUR** received the B.Tech. degree in electrical engineering from MIT, Muzaffarpur, India, in 1997, the M.Tech. degree in electrical engineering from RVDU, Udaipur, India, in 2008, and the Ph.D. degree in electrical engineering from MNNIT, Allahabad, India, in 2014. Currently, he is a Professor with the Department of Electrical Engineering, Graphic Era (Deemed to be University), Dehradun. He is an Associate Editor of IEEE ACCESS.



**KITMO** was born in Lokoro, Cameroon. He received the B.E. and master's degrees in electrical engineering from the University of Ngaoundere, Cameroon. He is currently a Teacher with the National Advanced School of Engineering of Maroua, Cameroon. Currently, he is working on the optimization of multi-source power plants for Smart Grids using artificial intelligence. He developed several models for the prediction of energy consumption in stand Alone and Grid-connected systems. This aspect of energy control is focused on the reduction of total harmonics of distortion (THD) and the design of multicellular active filters dedicated to high-voltage systems. His current research interests include renewable energy, smart grids, and embedded systems.

...